remote sensing

MDPI

Article

Detecting, Analyzing, and Predicting Land Use/Land Cover (LULC) Changes in Arid Regions Using Landsat Images, CA-Markov Hybrid Model, and GIS Techniques

Salman A. H. Selmy [1,*], Dmitry E. Kucher [2], Gintautas Mozgeris [3], Ali R. A. Moursy [4], Raimundo Jimenez-Ballesta [5], Olga D. Kucher [6], Mohamed E. Fadl [7] and Abdel-rahman A. Mustafa [4]

1 Department of Soils and Water, Faculty of Agriculture, Assiut University, Assiut 71526, Egypt
2 Department of Environmental Management, Institute of Environmental Engineering, People's Friendship University of Russia Named after Patrice Lumumba (RUDN University), 6 Miklukho-Maklaya St., 117198 Moscow, Russia; kucher-de@rudn.ru
3 Department of Forest Sciences, Agriculture Academy, Vytautas Magnus University, Studentų Str. 11, LT-53361 Akademija, Kaunas Dstr., Lithuania; gintautas.mozgeris@vdu.lt
4 Department of Soil and Water, Faculty of Agriculture, Sohag University, Sohag 82524, Egypt; ali.refaat@agr.sohag.edu.eg (A.R.A.M.); a_mustafa32@agr.sohag.edu.eg (A.-r.A.M.)
5 Department of Geology and Geochemistry, Autónoma University of Madrid, 28049 Madrid, Spain; raimundo.jimenez@uam.es
6 Scientific Department, Rural Urban Framework Center, People's Friendship University of Russia Named after Patrice Lumumba (RUDN University), 6 Miklukho-Maklaya St., 117198 Moscow, Russia; kucher-od@rudn.ru
7 Division of Scientific Training and Continuous Studies, National Authority for Remote Sensing and Space Sciences (NARSS), Cairo 11769, Egypt; madham@narss.sci.eg
* Correspondence: salman.selmy@agr.aun.edu.eg

Abstract: Understanding the change dynamics of land use and land cover (LULC) is critical for efficient ecological management modification and sustainable land-use planning. This work aimed to identify, simulate, and predict historical and future LULC changes in the Sohag Governorate, Egypt, as an arid region. In the present study, the detection of historical LULC change dynamics for time series 1984–2002, 2002–2013, and 2013–2022 was performed, as well as CA-Markov hybrid model was employed to project the future LULC trends for 2030, 2040, and 2050. Four Landsat images acquired by different sensors were used as spatial–temporal data sources for the study region, including TM for 1984, ETM+ for 2002, and OLI for 2013 and 2022. Furthermore, a supervised classification technique was implemented in the image classification process. All remote sensing data was processed and modeled using IDRISI 7.02 software. Four main LULC categories were recognized in the study region: urban areas, cultivated lands, desert lands, and water bodies. The precision of LULC categorization analysis was high, with Kappa coefficients above 0.7 and overall accuracy above 87.5% for all classifications. The results obtained from estimating LULC change in the period from 1984 to 2022 indicated that built-up areas expanded to cover 12.5% of the study area in 2022 instead of 5.5% in 1984. This urban sprawl occurred at the cost of reducing old farmlands in old towns and villages and building new settlements on bare lands. Furthermore, cultivated lands increased from 45.5% of the total area in 1984 to 60.7% in 2022 due to ongoing soil reclamation projects in desert areas outside the Nile Valley. Moreover, between 1984 and 2022, desert lands lost around half of their area, while water bodies gained a very slight increase. According to the simulation and projection of the future LULC trends for 2030, 2040, and 2050, similar trends to historical LULC changes were detected. These trends are represented by decreasing desert lands and increasing urban and cultivated newly reclaimed areas. Concerning CA-Markov model validation, Kappa indices ranged across actual and simulated maps from 0.84 to 0.93, suggesting that this model was reasonably excellent at projecting future LULC trends. Therefore, using the CA-Markov hybrid model as a prediction and modeling approach for future LULC trends provides a good vision for monitoring and reducing the negative impacts of LULC changes, supporting land use policy-makers, and developing land management.

Citation: Selmy, S.A.H.; Kucher, D.E.; Mozgeris, G.; Moursy, A.R.A.; Jimenez-Ballesta, R.; Kucher, O.D.; Fadl, M.E.; Mustafa, A.-r.A. Detecting, Analyzing, and Predicting Land Use/Land Cover (LULC) Changes in Arid Regions Using Landsat Images, CA-Markov Hybrid Model, and GIS Techniques. *Remote Sens.* **2023**, *15*, 5522. https://doi.org/10.3390/rs15235522

Academic Editor: Luis A. Ruiz

Received: 24 September 2023
Revised: 12 November 2023
Accepted: 24 November 2023
Published: 27 November 2023

Keywords: remote sensing; LULC classification; LULC changes; CA-Markov model; LULC projection; land-use planning; GIS; IDRISI

1. Introduction

Land degradation is a global issue caused by demographic growth, inappropriate land management, deforestation, climate change, and others [1]. Recently, Egypt has experienced a very complicated dynamic built-up sprawl process due to the fast population increase, which is the key driver of urbanization and LULC changes in arid lands, converting productive agricultural lands to urbanized areas, prompting concern among researchers [2]. Furthermore, in Egypt, growing urbanization is linked with population increases, resulting in intense farming land use to fulfill food demand. Accordingly, some Nile Valley and Delta fertile soils have been vulnerable to degradation and have lost their fertility and productivity. Hence, the sustainable development of current agricultural lands with an expansion of reclaimed soils is necessary to achieve food security, which has become the primary concern [3]. Land reclamation programs for arable land outside the Nile Valley have accelerated rapidly, aiming to increase farmed areas while relieving the pressure on fertile agricultural soils [4]. Thus, for Egypt, as an arid region, the detection and projecting of LULC changes are essential for long-term management and land-use planning of natural resources.

Many factors influence LULC changes, including time, scale, politics, economics, and social and cultural factors [5]. At all spatial–temporal scales, LULC changes have been recognized as significant drivers of environmental changes [6]. Such changes, along with other negative changes (e.g., climate change, biodiversity loss, and water, soil, and air pollution), should be the top priorities for humans [7]. Therefore, studying and monitoring the changes in LULC over time is both urgent and necessary to obtain an accurate future vision for sustainable development. Monitoring and relieving the unfavorable consequences of LULC dynamics while sustaining essential resource generation has, thus, become a top emphasis for researchers and policy-makers worldwide. Land use and land cover (LULC) describe the physical land types such as forests, wetlands, impervious surfaces, agriculture, water types, and others, as well as how humans use these land types in a region. Furthermore, LULCs are spatially dispersed due to the dynamic interactions between human activities and natural factors of ecosystems [8–11]. Natural, social, and economic variables all influence the complex dynamics of LULC systems. Changes in LULC availability and distribution have a substantial influence on climate, environmental challenges, and natural ecosystem conditions [12–14]. Furthermore, changes in global LULC are a major cause of significant concern for future LULC trends [15–19]. Moreover, LULC changes are a critical aspect of sustainability and management of natural resources [20–23].

In many cases, human activities have unfavorable impacts on LULC in diverse territories of the world. Human-induced LULC changes are driven mainly by the requirements of communities for food and economic development due to the rapidly increasing population growth globally [24–28]. These LULC shifts, however, have severe consequences for climate change, environmental conservation, environmental pollution, soil erosion, agricultural land production, biodiversity, and water resources [29–37]. In the investigation region, as arid land, the main driver of LULC changes is human activities due to population increase. This is similar to the rest of Egypt, which requires supporting economic development to meet food and housing requirements.

Above all, understanding and identifying detailed historical and future LULC dynamics knowledge over a lengthy series of periods and analyzing their patterns and processes is critical for land development decision-makers and planners. LULC changes are rapidly dynamic processes worldwide. Thus, it is widely recognized that LULC trends documenting and modeling improve knowledge of historical and future LULC patterns and their repercussions and guide future land-use planning [27,38,39].

Geographic information systems (GIS) and remote sensing (RS) techniques provide helpful approaches for understanding, analyzing, and monitoring LULC over time in landscapes [40,41]. Many investigations on LULCs have been conducted using these tools [42–45]. Additionally, Landsat periodic imagery data for a specific area is a reliable data source that can be utilized to forecast LULC trends in that area. GIS and RS techniques are effective for displaying spatial modeling methods [46]. Thus, modeling, simulation, and predicting the LULC changes using temporal–spatial data are crucial for improving LULC planning and management. Although the complexity of developing models and simulations is great, they are necessary to detect the LULC changes and analyze the causes and consequences of this phenomenon [47]. Furthermore, various approaches for determining historical and prospective LULC have been established to assist stakeholders in economic improvement, land conservation, and land-use planning. In addition, several models for simulating future scenarios of LULC have been created. These models deliver appropriate approaches for detecting the spatial variability patterns in LULC. Moreover, model validation is required for an accurate assessment of LULC prediction in a particular area by comparing predicted and observed LULC changes [48].

The combined Cellular Automata (CA) and Markov Chain model (CA-Markov Model) is one widespread model used with high accuracy for analyzing LULU dynamics [27,36,49]. Furthermore, the CA-Markov model's robustness provides an opportune manner for modeling LULC change dynamics spatially and temporally in complex landscapes [50–52]. The flexibility of the CA-Markov hybrid model to combine spatial and remote sensing data, as well as biophysical and socio-economic data, promotes a more extensive, detailed, and accurate projection of LULC change transitions [53]. Several studies have employed this model successfully in LULC prediction, e.g., [36,54–58]. CA-Markov hybrid model, which was employed in the present investigation, is an effective and widely used model among several models by researchers to detect, predict, monitor, and simulate spatiotemporal change in LULC [59–62].

The most significant stage in the CA-Markov model is the rules of transition, which depend on the training data [63]. Furthermore, the applied model is affected by neighborhood class and cell size, which are also considered in obtaining optimum simulation or prediction outcomes [13]. CA-Markov hybrid model can effectively incorporate remotely sensed data and GIS. This model can convert the results into spatially explicit results necessary for LULC development [64]. For simulating and predicting land-use changes, several modeling approaches are used [65]. Some of them are applied based on the statistical matching approach of the spatio-temporal data using the main variables of prediction. The others utilize algorithms specifically designed to assess human–environment interactions [66]. However, the Markov model is the earliest statistical model that can be generated with minimal input data [67,68]. In the current study, assessing and analyzing historical LULC change patterns from 1984 to 2022 and simulating and predicting future LULC trends of 2030, 2040, and 2050 in the study area using the CA-Markov model is beneficial for implementing sustainable land management [69]. Furthermore, there is a scarcity of research on detecting LULC and forecasting future scenarios in LULC in arid lands such as the study region. Therefore, the main goal of this work was to detect, analyze, and evaluate the historical change dynamics in LULC from 1984 to 2022 and to simulate and predict LULC trends for 2030, 2040, and 2050 using CA-Markov spatial modeling.

2. Materials and Methods

2.1. Study Area

In the current study, Sohag Governorate represents the arid land study area. Sohag Governorate is located in Upper Egypt and encompasses a portion of the Nile Valley beside the eastern and western desert belts. It has an area of around 11,120 km^2 and a population of 5.45 million in 2021. The Nile River runs for about 125 km through the Sohag Governorate. The study region is situated at latitudes of 26°07′ and 26°57′N, as well as longitudes of 32°14′ and 31°20′E, and it is bounded on the south by Qena Governorate and on the north by Assiut Governorate (Figure 1). Climatically, the research region is located in North Africa's arid region, which is characterized by hot summers and mild winters with extremely low to nil rainfall. The monthly averages of temperatures, evaporation, and rainfall data for the study region are depicted in Figure 2. Temperature varies from 15.5 °C to 36.5 °C, and the relative humidity ranges between 35% and 61%. Following Soil Survey Staff [70], *Hyperthermic* is the soil temperature regime, and *Toric* is the moisture regime. The study area includes four LULC categories: urban areas; cultivated lands; deserts; and water bodies, as shown in Table 1.

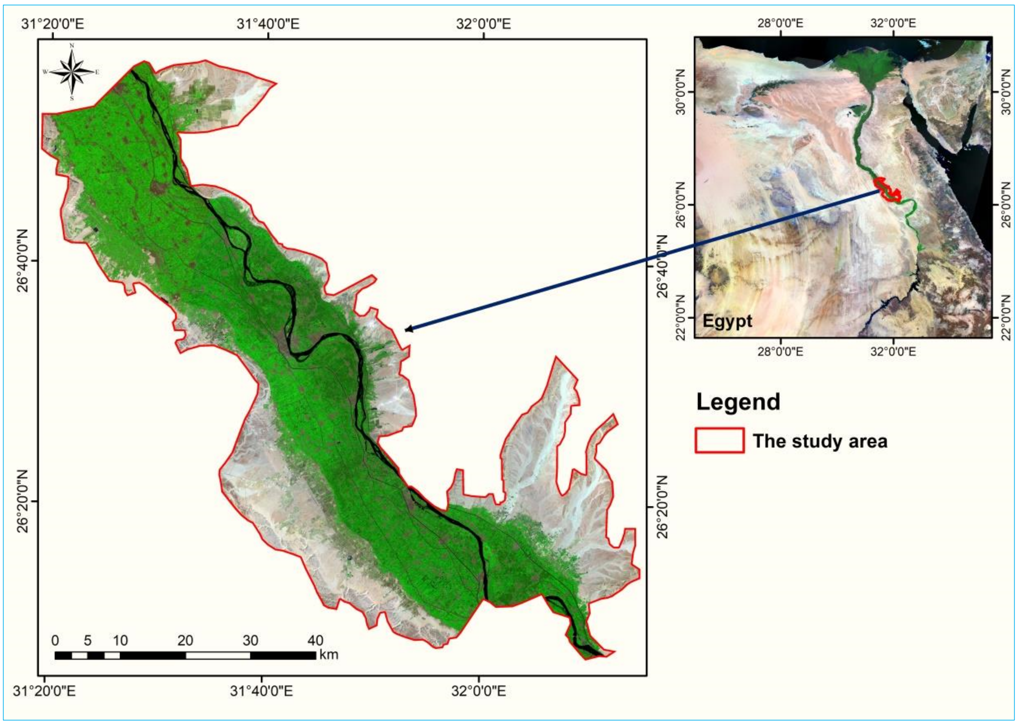

Figure 1. Map of the investigation region.

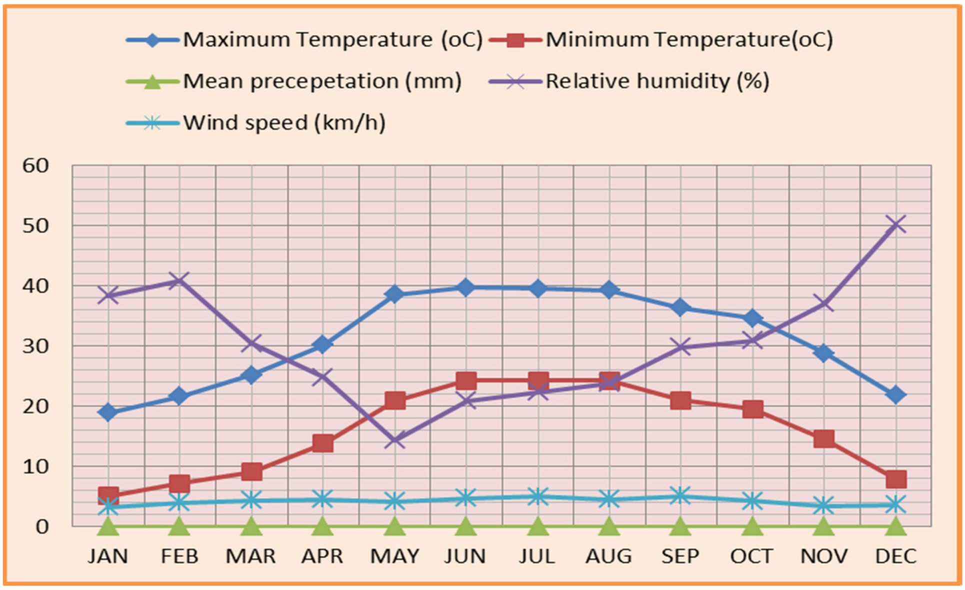

Figure 2. Climate data for the study region.

Table 1. Types of LULC in the study site.

LULC	Description
Water bodies	The Nile River, canals, drainage patterns, and wastewater treatment plants.
Desert lands	Bare lands, sand sheets, and rocky lands in the eastern and western parts outside the Nile Valley.
Cultivated lands	Old cultivated lands in the Nile Valley and newly reclaimed lands outside the Nile Valley.
Urban areas	Residential, commercial, industrial, and road constructions in cities and rural areas.

2.2. Data Acquisition

Remotely sensed and spatial data are trustworthy data for detecting and comprehending the dynamic causes of LULC in any terrain [71]. The primary remotely sensed and ancillary data utilized in this work were four multispectral images of Landsat. These images were acquired by the thematic mapper (TM), the enhanced thematic mapper (ETM+), and the operational land imager (OLI) sensors for the years 1984, 2002, 2013, and 2022, respectively. Each of the four images used was created by mosaicking three adjacent captured images to cover the investigation region. The four images' geo-coded cloud-free digital data were obtained from the Landsat archive of the United States Geological Survey (USGS) (https://earthexplorer.usgs.gov, accessed on 5 January 2022). The principal specifications of the images used are shown in Table 2. The study site boundary was subsetted using topographic maps at 1:50,000 scales obtained from the Egyptian Survey Authority (ESA) as a reference. For creating the digital elevation model (DEM), Advanced Spaceborne Thermal Emission and Reflection Radiometer (ASTER) data were used after radiometric and geometric corrections, as described in Table 3. Figure 3 displays the created DEM.

Table 2. The principal specifications of the used Landsat satellite images.

Satellite Image	Year of Acquisition	Path/Row	Resolution (m)	Image Type
Landsat 5 (TM) Landsat 7 (ETM+) Landsat 8 (OLI) Landsat 9 (OLI)	1984 2002 2013 2022	175/42, 176/42 and 176/41	15–30	Level-1

TM = thematic mapper. ETM+ = enhanced thematic mapper. OLI = operational land imager.

Table 3. The specifications of the ASTER utilized.

Sensor	Spectral Range	Bands	Resolution (m)	Swath Width (km)	Quantization Level (Bits)
ASTER	VNIR, SWIR, and TIR	14	15–90	60	8–12

VNIR = visible and near-infrared. SWIR = short-wave infrared. TIR = thermal infrared.

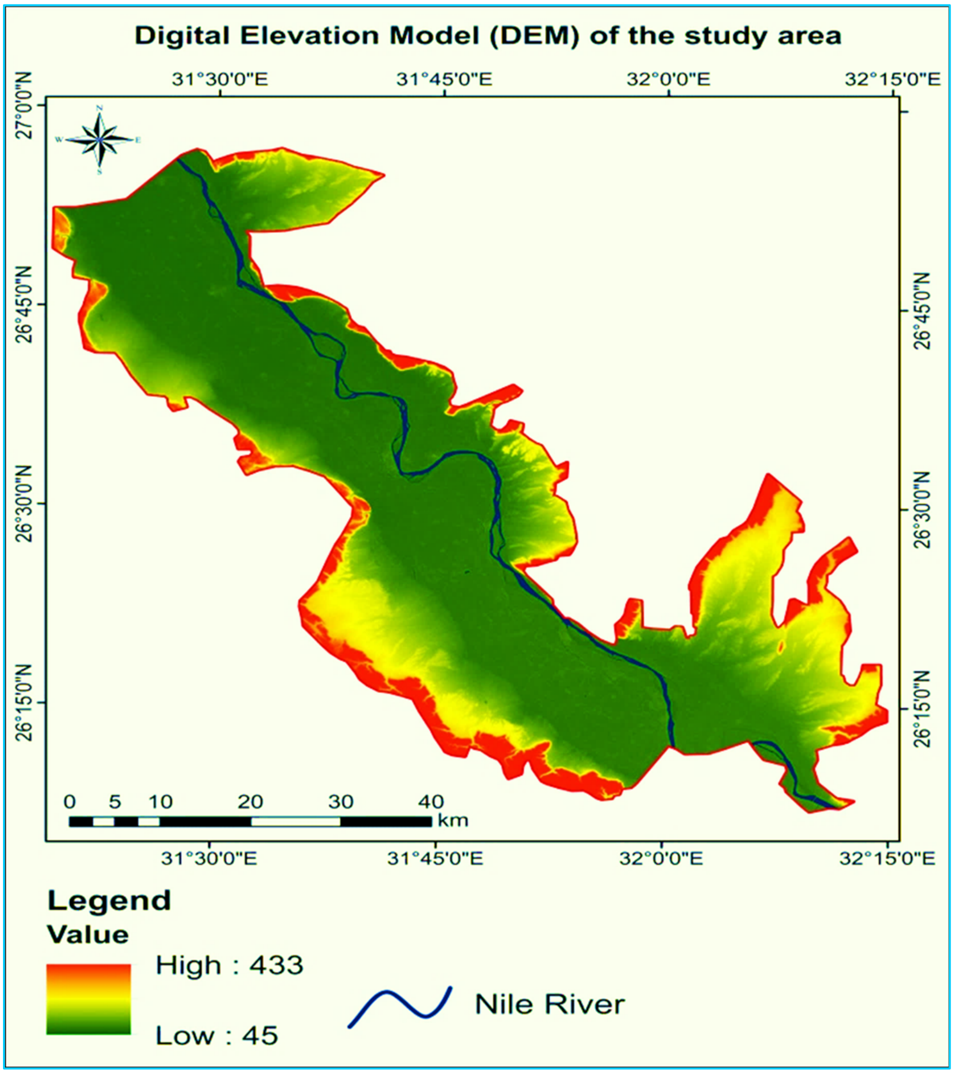

Figure 3. Digital elevation model (DEM) map generated from ASTER data.

2.3. Pre-Processing of Remote Sensing Data

Pre-processing remotely sensed data is required to reduce noise, prepare the data, and increase its suitability for further analysis. As previously stated, three images were employed to cover the study area, totaling twelve images covering the investigated time series from 1984 to 2022. Using the ENVI platform, all Landsat images underwent pre-processing, including layer stacking, geometric correction, mosaicking, and band extraction. First, the multi-temporal Landsat images were imported into the ENVI platform, and all spectral bands were layer-stacked. Concerning the geometric correction process, the entire datasets employed were resampled and projected to the World Geodetic System 1984 (WGS84) into the Universal Transverse Mercator (UTM), with a root mean square error (RMSE) of less than 0.5 pixels [43,72]. For all images of interest, a standard geographic coordinate system was used throughout the geometric rectification process. Furthermore, choosing ground control points (GCPs) is critical for geometric rectification. The digital data for 1984 were registered using 50 GCPs that were easily identifiable on both satellite images and on the ground (map-to-image registration). In addition, the first polynomial order and nearest neighborhood resampling approaches were used to set the pixel size at 30 m for image registration. The remaining images were rectified (image-to-image registration) using the corrected image of 1984 as a reference, following the same resampling method. Furthermore, the nearest neighborhood algorithm was applied over images for the resampling process without changing the original brightness magnitudes of pixels.

Before image classification, the temporal images must be radiometrically adjusted to normalize brightness variations induced by changing atmospheric conditions. Radiometric normalization was performed on the images using pseudo-invariant features (PIFs), which are spatially well-defined, spectrally stable, and radiometrically stable features. The image with the highest dynamic brightness value range, i.e., 2013, was chosen as a reference or base image for radiometric correction of other images from 1984, 2002, and 2022.

2.4. Image Classification and Accuracy Assessment

The main targeted LULC categories in the study site were built-up areas, cultivated lands (old farmlands and newly reclaimed farmlands), deserts, and water bodies. In terms of image classification, each image was classified individually before extracting primary LULC maps. Furthermore, image classification was performed employing supervised classification. For image classification, a decision tree classifier (DTC) approach was applied to integrate different remote sensing-derived indices. The DTC is defined as a machine-learning-based analysis technique comprising several classes of modeling algorithms using a tree structure, in which each node shows a test on attributes; the branch represents the test results, and the leaf node shows the target classes. In addition, the DTC is a multistage classifier that can be applied to a single image or a stack of images. It comprises a series of binary decisions to place pixels into classes. Each decision divides the pixels of the image into two categories based on the expression. Furthermore, the DTC is a hierarchical model composed of decision rules that recursively split independent variables into homogeneous zones. Therefore, we used it to determine the correct category for each pixel, with certain classes being separated during each step in the simplest manner possible (Figure 4). The DCT has been widely used for land cover classification, particularly with remote sensing technology approaches, and is often used to integrate multi-source data. In practice, the DTC concept is often translated using classification rules. Three stages are used to build the classification rules, including the following: (1) generating and perfecting knowledge and rules from experts; (2) extracting variables and rules using cognitive methods; and (3) automatically generating rules from observed data. As a result, the LULC in the study area is categorized into four LULC categories: urban areas; cultivated land; deserts; and water bodies, as defined in Table 1. The Normalized Difference Vegetation Index (NDVI), Modified Normalized Difference Water Index (MNDWI), Normalized Difference Built-Up Index (NDBI), and Dry Bare Soil Index (DBSI) were among the indices utilized. These indices were chosen according to the diverse land uses in the study area and were employed to improve the precision of the image classification process. The expressions of all indices utilized are shown in Table 4.

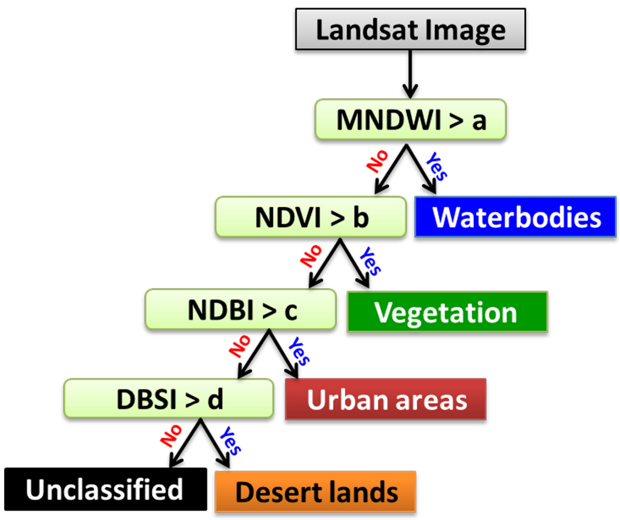

Figure 4. Decision tree for the LULC classification in the study area.

Table 4. The applied indices expressions.

The Index	Expression	Reference
NDVI	(NIR − R)/(NIR + R)	[73]
MNDWI	(G − SWIR)/(G + SWIR)	[74]
NDBI	(SWIR − NIR)/(SWIR + NIR)	[75]
DBSI	[(SWIR)/(SWIR + G)] − [(NIR − R)/(NIR + R)]	[76]

NIR = near-infrared. SWIR = short-wave infrared. R = red. G = green.

Accuracy evaluation processes decide the reliability of the spatial information generated from remote sensing images for accurate image classification [77,78]. Remotely sensed spatial information is both reliable and accurate when used in integration with ground control points that serve as a reference [79]. The preliminary geomorphologic units of the Sohag Governorate area were identified and verified through field observations after visual interpretation of satellite Landsat images. In this work, the accuracy of images from 1984, 2002, 2013, and 2022 was assessed using the visual interpretation of Landsat images [80]. A semi-detailed survey was completed in 2022 to obtain more detailed spatial information about the soil patterns, landforms, and landscape characteristics as ground truth data throughout the investigated area. Moreover, various statistical methods of the error matrix can be used for accuracy assessment [81]. Therefore, the accuracy of each categorized image was determined and evaluated by calculating the producer's accuracy, user's accuracy, overall accuracy, and Kappa coefficient values, as described in Equations (1)–(4) [79,82,83]. Furthermore, due to the nature of GIS and its integration with remote sensing (RS), the combination of GIS, RS data, and the Markov model was supported [53,84]. Therefore, thematic maps of different LULC for studied periods were created using ArcGIS 10.8 software.

$$A_p = p_{ii}/P_{+i} \tag{1}$$

$$A_u = p_{ii}/P_{i+} \tag{2}$$

$$A_O = \frac{\sum_{i=1}^{m} p_{ii}}{n} \times 100 \tag{3}$$

$$k = \frac{\mathrm{n}\sum_{i=1}^{m} \mathrm{p_{ii}} - \sum_{i=1}^{c} p_{i+}p_{+i}}{\mathrm{n}^2 - \sum_{i=1}^{m} p_{i+}p_{+i}} \tag{4}$$

where A_p is the accuracy of the producer; A_u is the accuracy user; A_o is the overall accuracy; K is the kappa coefficient; p_{ii} is the percentage of zones of categorized and reference categories, and P_{+i} = P_{i+} = $\sum_{i=1}^{m} p_{ii}$ is the percentage of zones of categorized categories and ground truth categories.

2.5. LULC Change Analysis Using CA-Markov Modeling

CA-Markov hybrid model was employed to simulate future LULC trends in this study. Using transition probability, the CA-Markov hybrid model, as a separate random process, forecasts the next scenario of LULC and all future scenarios depending on the current situation [85]. Furthermore, the CA-Markov analysis technique is a simple statistical tool that employs a transition probability matrix depending on the influences of the neighborhoods via a spatially influenced algorithm [86,87]. The CA-Markov hybrid model has been extensively and increasingly utilized in LULC prediction in recent years because of its ability to fit the complicated spatial nature [47,88–91]. However, the matrix of transition probability of each LULC class may be accurate, but the spatial distribution of the occurrences is unknown [46]. This is because the Markov chain model has a deficiency in projecting the spatial assignment and distribution of LULC categories [92]. Therefore, to fill this gap, the CA-Markov hybrid model was developed to enhance the precision of the change detection of different land-use categories by providing spatial dimension via cellular automata (CA) filter to the used model [93,94].

The cellular automaton (CA) model assumes that a grid cell's states are determined by the changes (dynamics) of the cell itself and its neighbors' grid cells [95,96]. Thus, a hybrid Markov–Cellular Automata model can be applied to detect the spatial and temporal changes in the Sohag Governorate's different land uses with a dynamic degree of estimation by setting a dataset of land uses at a specific time, then projecting the changing probabilities of these data for a future time [43,90]. Change detection in LULC changes, on the other hand, is accomplished by predicting changes in satellite image pixels from one land-use category at a time (t1) into the other at a time (t2). Equations (5)–(7) express the employed models [97].

$$P_{ij} = \begin{bmatrix} P_{11} \; P_{12} \ldots \; P_{1n} \\ P_{21} \; P_{22} \ldots \; P_{2n} \\ P_{n1} \; P_{n2} \ldots \; P_{nn} \end{bmatrix} \tag{5}$$

$$0 \le P_{ij} < 1 \; and \sum_{j=1}^{n} P_{ij} = 1, i, j = 1, 2, \ldots, n \tag{6}$$

$$S_{t+1} = P_{ij} \times S_t \tag{7}$$

where P_{ij} is the transitional probability matrix of changing from a specific land use studied (n) to another, and its value ranges from 0 to 1; S_t is the current land-use status at time t, and S_{t+1} is the next land-use state at time t + 1. To obtain both the transition and probability matrix of LULC types, CA-Markov Chain analysis was performed using IDRISI 7.02 software for the 1984–2002, 2002–2013, and 2013–2022 time series.

2.6. Future LULC Prediction for 2030, 2040, and 2050

Markov Chain model, when combined with Cellular Automata, offers an excellent chance to forecast and simulates the spatial–temporal LULC changes. Furthermore, this integrated approach is also effective in modeling and forecasting the complex LULC categories [50,52,98]. Therefore, the CA-Markov hybrid model with two variables was employed in the process of LULC simulation and prediction. The two variables used are the discrete variable in time and space and the local variable, which they usually allocate to interactions [99]. Grid sizes, cell neighborhoods, cell spaces, time phases, and transition rules are the core components of the CA-Markov hybrid model [100,101]. Cells are objects in any dimensional space that are adjacent or close to one another. Each cell can only be in one of the states that define the system's attributes at a time. The state of any cell is determined by the states of other cells in its neighborhood, defined as the immediately adjacent set of cells that are "next" to the cell in question. Finally, transition rules drive changes in the state of each cell as a function of what exists or is happening in the cell's vicinity. Employing the inter-period change–transition probability matrix, the CA-Markov hybrid model integrates the idea of projecting the next time state depending on the previous period states [102,103]. Furthermore, this model can determine neighbors, and the greater the weight factor, the closer the distance between cells and their neighbors [43,90]. Therefore, the weight factor and transition probability can forecast the states of neighbor grid cells [44]. The land-use changes were calculated using Equation (8).

$$Si = \frac{LU_{(i,\,t2)} - LUA_i}{LU_{(i,\,t1)}} \times \frac{1}{t_2 - t_1} \times 100\% \tag{8}$$

where Si is land-use change; $LU_{(i,t1)}$ is land-use change at an earlier period; $LU_{(i,t2)}$ is land-use changed area at a later period, and LUA_i is the area with no change.

Future LULC trends for future dates studied were projected based on the historical patterns (from 1984 to 2022) in the study area. CA-Markov was employed in IDRISI 7.02 software to forecast the future LULC trends in 2030, 2040, and 2050. In the present study, LULC images of the Sohag Governorate area over two-time series in 1984 as earlier land-use (t1) and 2022 as later land-use (t2) were utilized, as described by Hyandye and Martz [50]. A standard contiguity filter (5 × 5 pixels) was applied to the images to identify the neighborhood cells of each land-use class. To achieve a good influence, each cell was surrounded by a matrix scope of 5 × 5 cells. This spatial filter occurs near an existing category and rules out changes in land use randomly [104]. Furthermore, the pixels close to the existent LULC class are more suitable than those far away [105]. In the current study, neighboring pixels were utilized to generate spatially neighboring weights to project LULC categories for 2030, 2040, and 2050. The contiguity filter used for LULC change analysis is shown below (Equation (9)).

$$\text{Contiguityfilter } 5 \times 5 = \begin{bmatrix} 0\,0\,1\,0\,0 \\ 0\,1\,1\,1\,0 \\ 1\,1\,1\,1\,1 \\ 0\,1\,1\,1\,0 \\ 0\,0\,1\,0\,0 \end{bmatrix} \quad (9)$$

The methodology of analyzing, simulating, and projecting LULCs employing the CA-Markov hybrid model is summarized into four main steps, which are as follows:

1. The Markov chain model was used to compute transition probabilities matrices for 1984, 2002, 2013, and 2022;
2. The computed transition matrices were used to generate a set of conditional probability data for the different land uses from 1984 to 2022;
3. The transition probabilities matrices of 1984–2002, 2002–2013, and 2013–2022 for each LULC category, as well as conditional probability data and LULC, classified maps of 2013 and 2020, were integrated using the CA-Markov spatial operator in IDRISI 7.02 software, which is based on Markov chain analysis and multi-criteria evaluation (MCE), to simulate the LULC maps of 2030, 2040, and 2050;
4. Predicted LULC maps for future dates were produced by overlapping the results obtained in the previous steps.

2.7. CA-Markov Model Validation

According to Eastman [106], the utility of any predictive change model is dependent on the outcome of the validation process. The CA-Markov model outputs had to be validated before modeling the future LULC trends for 2030, 2040, and 2050. Therefore, the CA-Markov model was validated using the validation module in IDRISI 7.02 software to compare the degree of agreement between the predicted and the classified maps. The validation process was performed by comparing the LULC predicted results (projected maps) for 2013 and 2022 to their corresponding observed datasets (classified maps), which were used as LULC reference data. Furthermore, Kappa coefficients were calculated and utilized to evaluate the performance precision of the applied model in the LULC projection maps. The current study applied the statistic Kappa indices, including the Kappa for no information (K_{no}), Kappa for location ($K_{location}$), Kappa for location strata ($K_{location\ strata}$), and Kappa standard ($K_{standard}$) [51,104]. Kappa statistical indicator can distinguish between quantity errors and location errors between two qualitative maps [52,107] and is computed employing Equation (10) [108].

$$Kappa = \frac{P_0 - P_C}{1 - P_C} \quad (10)$$

where P_0 is the portion of cells correctly classified, and P_C is the hypothetical probability of opportunity agreement between the actual LULC of 2013 and 2022 maps (Landsat images classification) and the projected LULC of 2013 and 2022 maps.

The employment of Kappa indices in the computation determines the overall accomplishment rate and provides insight into the true causes of the strength or weakness of the outcomes. The Kappa values were categorized according to Aliani et al. [93], as illustrated in Table 5. Furthermore, Figure 5 demonstrates the methodology for LULC analysis and LULC projection employing the CA-Markov hybrid model.

Table 5. Kappa coefficient values and agreement degrees.

Kappa Coefficient Value	Agreement Degree
<0.2	Weak
0.21–0.4	Acceptable
0.41–0.6	Moderate
0.61–0.8	Good
0.81–1.0	Very good

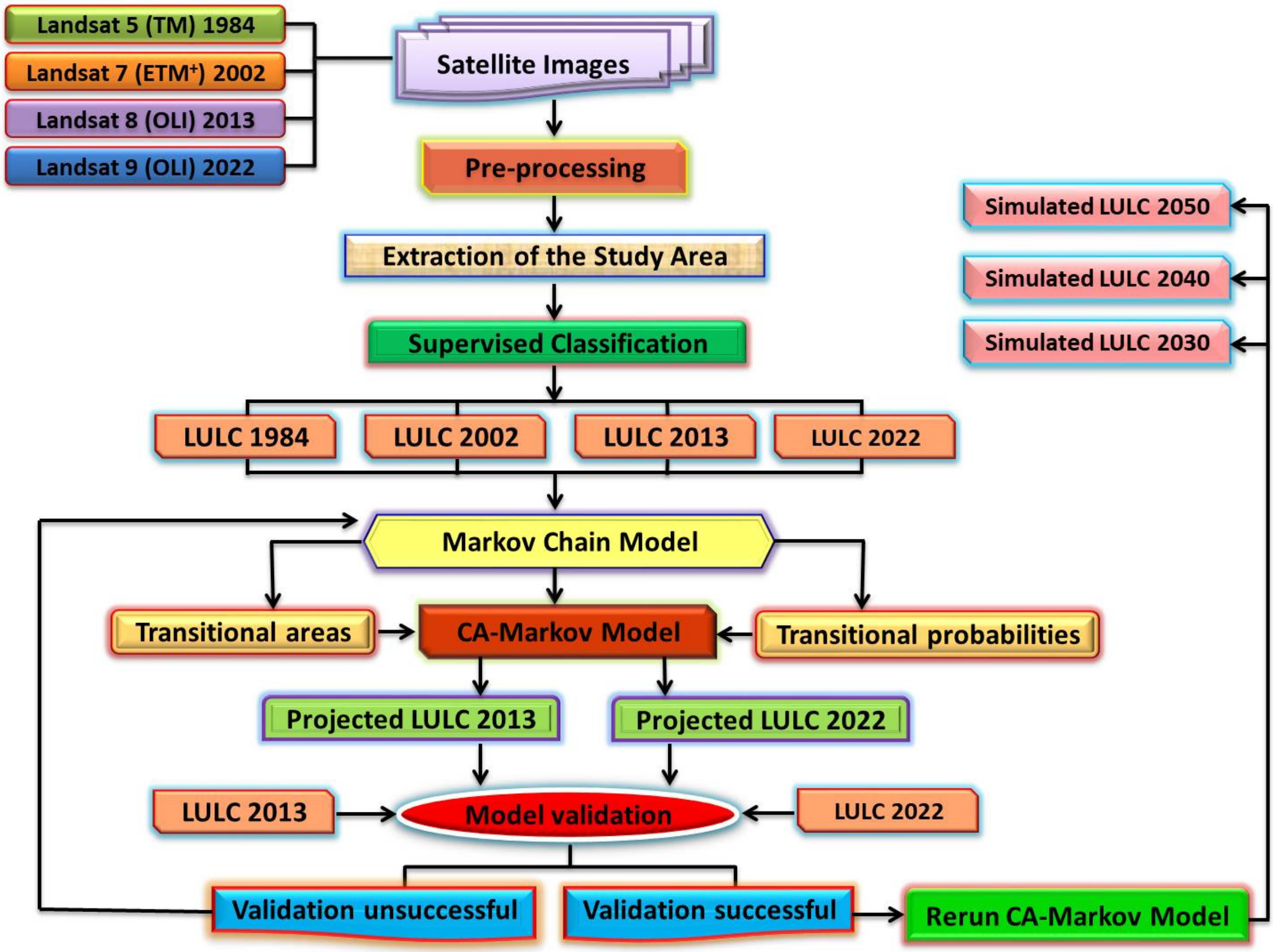

Figure 5. Simplified flowchart of LULC simulation methodology.

3. Results and Discussion

3.1. Accuracy Assessment of the LULC Classification

The obtained results showed that the overall accuracy and kappa statistics of all different land-use types in the Sohag Governorate area were acceptable for the different periods studied in 1984, 2002, 2013, and 2022 (Table 6). In the current study, the classification accuracy met the criterion that there must have been at least 80% accuracy for the sensor data [109]. The overall accuracy of the LULC classification ranged from 87.5% to 95.5% (Table 6). According to Anderson et al. [82], these percentages represent high accuracy; thus, the LULC maps can be utilized with reliability for LULC change dynamics analysis and forecasting. Furthermore, the kappa coefficient values indicated that the strength of agreement ranged from good to very good according to criteria adopted by Aliani et al. [93], as the Kappa coefficient values ranged from 0.71 to 0.95 (Table 6). Furthermore, Kappa values were described as a considerable agreement to near perfect agreement [98]. The assessment of overall accuracy and Kappa coefficient (Table 6) demonstrated the high capacity of the decision tree classifier (DTC) approach in integrating with different remote sensing-derived indices in producing multi-temporal LULC maps. Thus, this technique's findings are supposed to be compatible and reliable for modeling future LULC scenarios [27,110–112]. As a consequence, the categorized images are valid for examining and forecasting the changing dynamics of LULCs in the study area [50].

Table 6. Accuracy assessment of classified images for 1984, 2002, 2013, and 2022.

LULC Class	Landsat TM 1984		Landsat ETM$^+$ 2002		Landsat ETM$^+$ 2013		Landsat OLI 2022	
	PA	UA	PA	UA	PA	UA	PA	UA
	(%)							
Water bodies	97.1	100.0	99.4	98.9	98.7	96.3	82.2	97.4
Desert lands	99.7	91.1	97.8	99.2	96.4	92.5	88.6	45.9
Cultivated lands	72.2	91.2	91.7	86.4	86.1	95.5	94.6	92.3
Urban Areas	82.5	68.6	96.9	57.3	96.7	71.8	95.8	40.4
Overall accuracy	91.0		95.5		92.1		87.5	
Kappa coefficient	0.71		0.94		0.84		0.79	

PA = producer accuracy. UA = user accuracy.

3.2. The LULC Classification

According to the results of the maximum likelihood algorithm of Landsat images supervised classification, there were four LULC categories recognized in the study region: urban areas (residential, commercial, industrial, and road constructions); cultivated lands (old cultivated lands, and newly reclaimed lands); deserts (bare lands, sand sheets, and rocky land); and water bodies (the Nile River, canals, drainage patterns, and wastewater treatment plants). These findings are in line with earlier studies [113–121], which found the same LULC categories in other areas of Egypt, such as the Northwestern Coast, Nile Delta, and others. Table 7 displays the measurable data of the four LULC categories over the different time nodes. Furthermore, Figure 6 illustrates the spatial distribution of LULC types (classified maps) derived from satellite images of the Sohag Governorate area for the examined dates of 1984, 2002, 2013, and 2022. On the created maps, the different LULC categories were tagged with different colors.

The LULC class percentages of the total study area for 1984, 2002, 2013, and 2022 showed that deserts and cultivated lands were consistently the most extensive, followed by built-up and water bodies, which were far less extensive (Table 7). Similarly, previous investigations have reported that the LULC classes in the investigated areas of Egypt are dominated by deserts and cultivated regions [113,116,117,119]. Thus, in arid land regions, these LULC categories are dominant. Furthermore, throughout the 38 years from 1984 to 2022, the area of each LULC category in the Sohag Governorate changed significantly. According to the current study, cultivated lands and desert areas have been predominant from 1984 until 2022. According to Table 7, deserts and cultivated land constituted the majority of LULCs in the study region, accounting for 1398.9 km^2 (46.8%) and 1361.0 km^2 (45.5%) of the total area in 1984, respectively, and 703.8 km^2 (23.6%) and 1814.5 km^2 (60.7%) in 2022 (Figure 6). Moreover, urban and water bodies represented the lowest proportion of LULCs, as shown in Table 7. Also, urban areas more than doubled from 165 km^2 (5.5%) in 1984 to 369 km^2 (12.3%) in 2022 (Table 7).

Table 7. LULC classification for 1984, 2002, 2013, and 2022.

Land Use	1984		2002		2013		2022	
	Area							
	km^2	**%**	**km^2**	**%**	**km^2**	**%**	**km^2**	**%**
Water body	64.2	2.2	60.6	2.0	68.6	2.3	101.8	3.4
Desert lands	1398.9	46.8	1181.8	39.5	861.3	28.8	703.8	23.6
Cultivated lands	1361.0	45.5	1514.0	50.7	1754.7	58.7	1814.5	60.7
Urban	165.0	5.5	232.8	7.8	304.5	10.2	369.0	12.3
Total	2989.1	100.0	2989.1	100.0	2989.1	100.0	2989.1	100.0

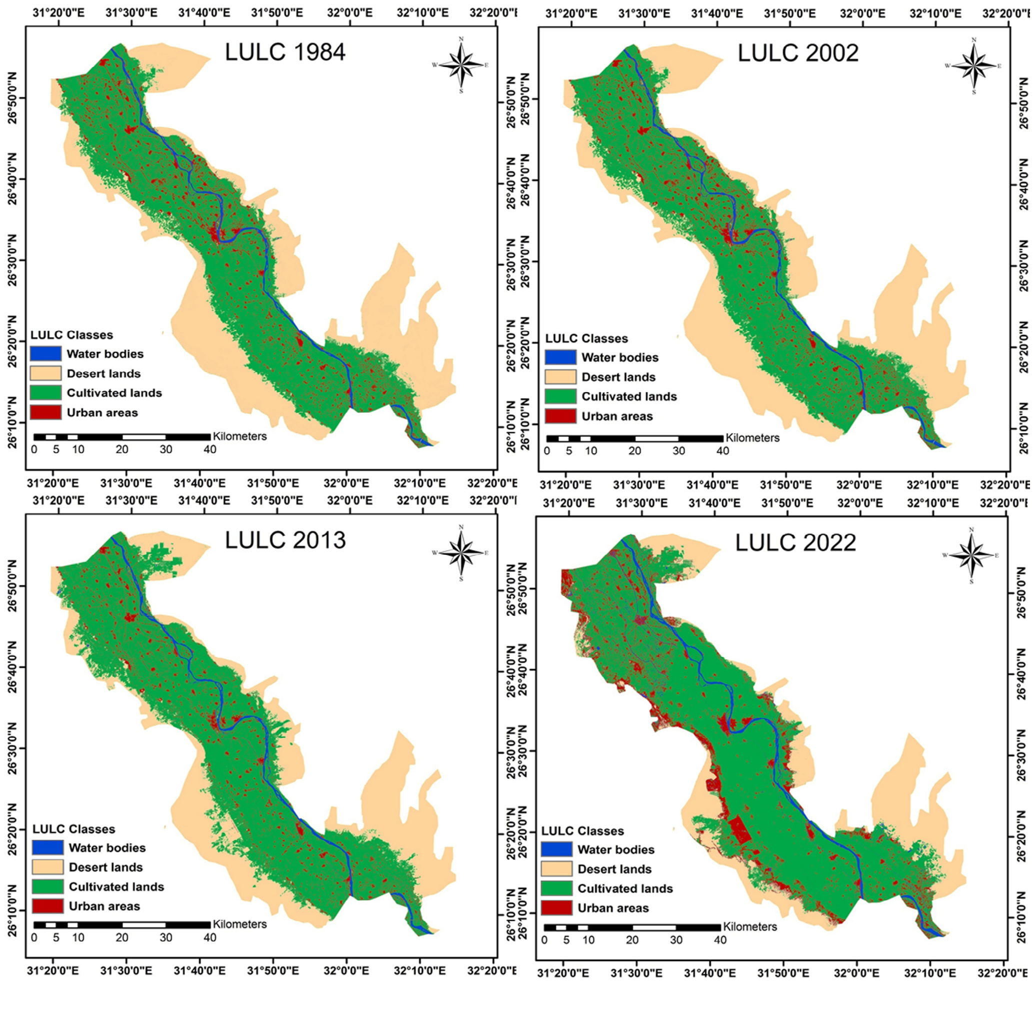

Figure 6. Classified maps of LULCs for 1984, 2002, 2013, and 2022.

3.3. LULC Change Dynamics

The results indicated that the built-up areas had a net gain of 67.74 km^2 between 1984 and 2002 due to the construction of new housing as the population increased (Figure 7). Similarly, cultivated lands have gained 152.99 km^2. Furthermore, during this period (1984–2002), many desert land areas were subjected to reclamation processes. As a result, cultivated lands increased while desert lands decreased. This is obvious in Figure 7, which showed a decrease in desert lands with a loss of 217.13 km^2. Concerning water bodies, some islands in the study area had vanished completely, while new islands had appeared in other locations. Furthermore, depositional processes cause the formation of new floodplains on the river's convex sides, as well as new islands and sand bars. As a result, between 1984 and 2002, the Nile River lost 3.6 km^2.

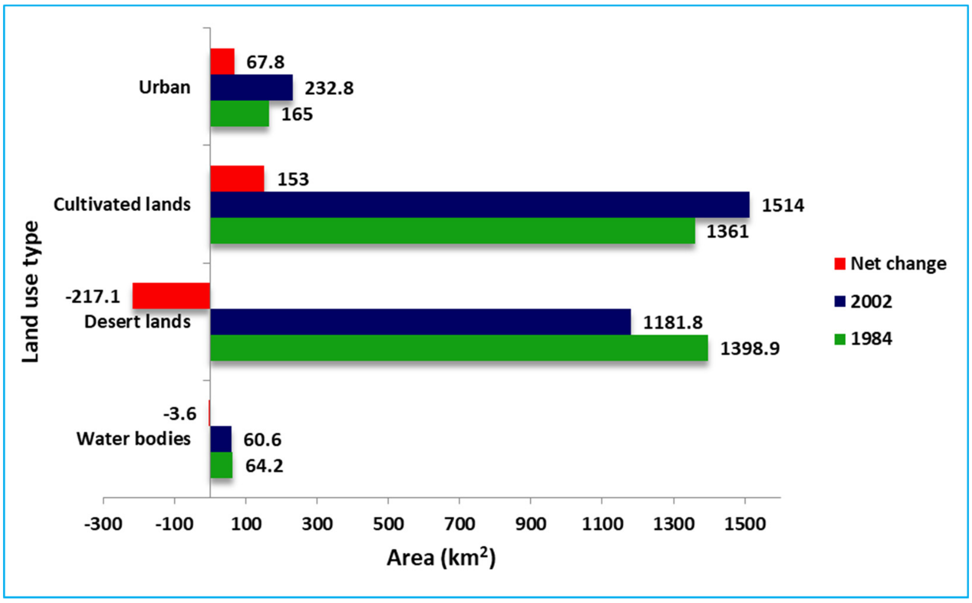

Figure 7. The changes in LULC categories between 1984 and 2002 (km^2).

During the time series from 2002 to 2013, water bodies in the study area increased by 8.04 km^2 (Figure 8). This could be attributed to the construction of numerous wastewater treatment plants. These treatment units are located on the outskirts of desert areas outside the Nile Valley. Furthermore, this treated wastewater is destined to irrigate crops, forest trees, decorative plants, and landscapes of greenbelts and is not intended for food. Moreover, soil reclamation activities increased dramatically during this period, consequently increasing cultivated lands by 240.73 km^2. Therefore, the desert lands had a net loss of 320.5 km^2 in the same period (2002–2013). Additionally, during this period, a substantial increase in built-up settlements occurred at the cost of the most productive land in the investigation area (Figure 8). According to Figure 8, there was a high sprawl rate of built-up areas on cultivated lands, which is one of the main problems that threaten the limited fertile lands in the Sohag Governorate. During this period (2002–2013), urban settlements expanded by 71.73 km^2. Figure 8 depicts the changes in LULC categories in the study area from 2002 to 2013.

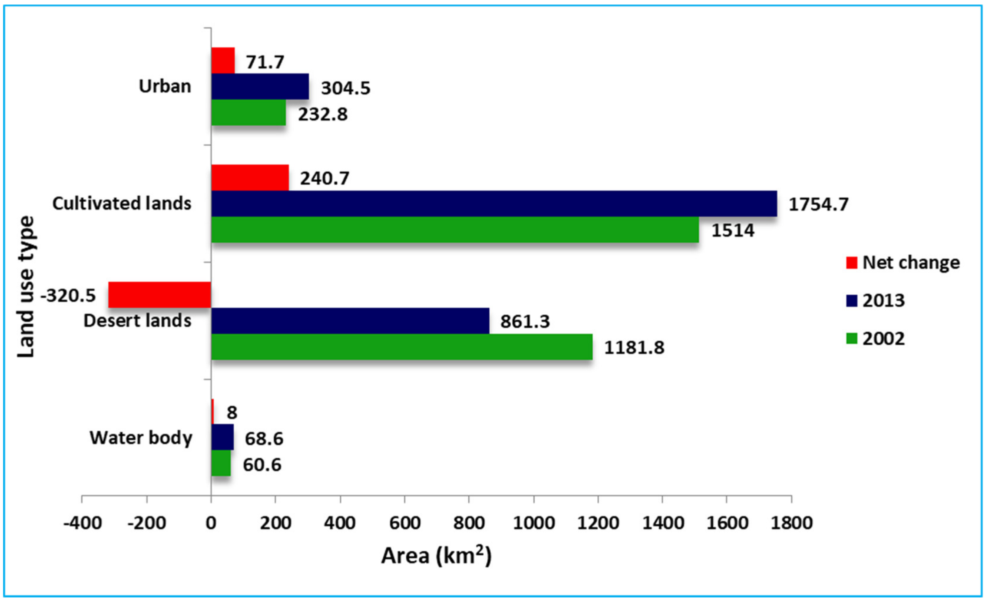

Figure 8. The changes in LULC categories between 2002 and 2013 (km^2).

During the third investigated period (2013–2022), water bodies in the study area increased by 33.21 km^2, as shown in Figure 9. At this period, the population of the Sohag Governorate was estimated to be around 5,193,052, accounting for 5.2 percent of the total population of Egypt. This could result in increased water consumption and, as a result, increased wastewater pumped to treatment plants. Both soil reclamation activities and urbanization increased during this period but to a lesser extent than in previous periods. The cultivated lands and urban areas recorded an increase of 59.73 km^2 and 64.52 km^2, respectively. In addition, the desert lands experienced a net loss of 157.47 km^2 (Figure 9).

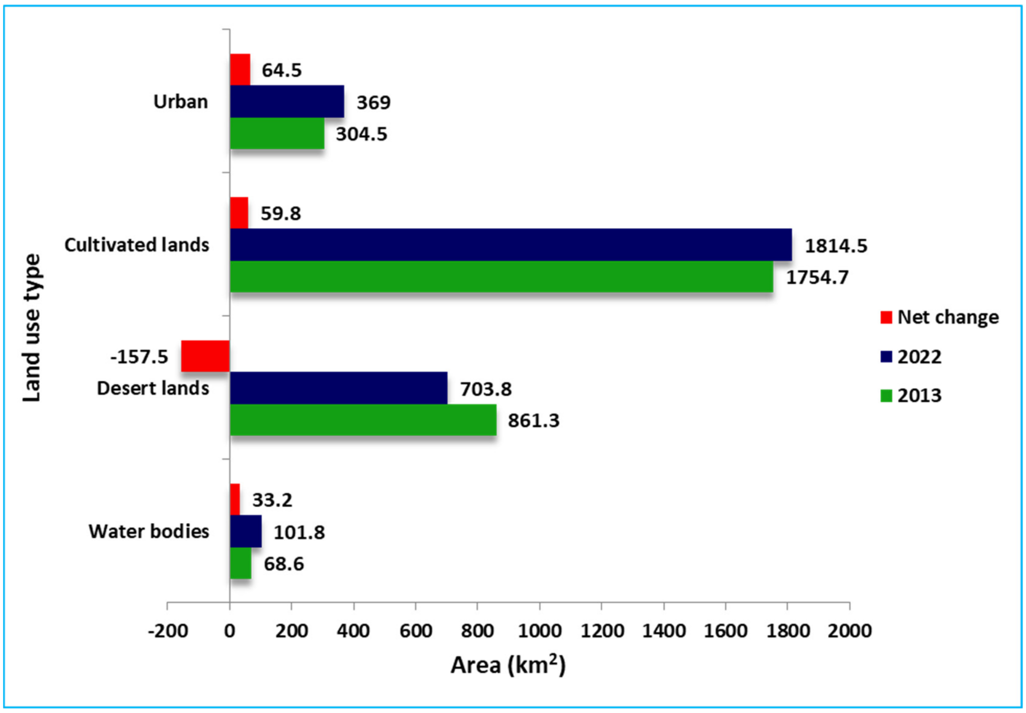

Figure 9. The changes in LULC categories between 2013 and 2022 (km^2).

Overall, the findings of this study revealed a continuous increase in urban sprawl and expansion of newly reclaimed cultivated lands, with a reduction in desert areas over the time series analyzed. These findings are in agreement with previous studies, which reported similar LULC change trends [113–121].

3.4. Markov Chain Model Analysis

The data displaying the decreases and increases in transition probabilities over time series from 1984 to 2022 are shown in Tables 8–10. The gains were acquired by subtracting the persistence from the entire column for each group, while the losses were received by deducting the persistence from the whole row [122]. For instance, the probability of remaining built-up areas as built-up areas from 1984 to 2002 is 69.75%, while the future change possibility of cultivated lands to urban areas is 20.36%, and so on for the rest of the LULC types. Desert lands and water bodies had high probabilities of 76.33 and 76.49%, respectively, as they did in 2002.

Table 8. Transition probability matrix derived from LULC-classified categories in Sohag Governorate from 1984 to 2002.

	Probability of Changing from 1984 to 2002				Subtotals	
	Water Bodies	**Desert Lands**	**Cultivated Lands**	**Urban Areas**	**Total**	**Loss**
Water bodies	0.7649	0.0005	0.1626	0.072	1	0.2351
Desert lands	0.0009	0.7633	0.2277	0.0081	1	0.2367
Cultivated lands	0.0043	0.0079	0.7842	0.2036	1	0.2158
Urban Areas	0.0356	0.2528	0.0141	0.6975	1	0.3025
Total	0.8057	1.0245	1.1886	0.9812	4	
Gain	0.0408	0.2612	0.4044	0.2837		

Table 9. Transition probability matrix derived from LULC-classified categories in Sohag Governorate from 2002 to 2013.

	Probability of Changing from 2002 to 2013				Subtotals	
	Water Bodies	**Desert Lands**	**Cultivated Lands**	**Urban Areas**	**Total**	**Loss**
Water bodies	0.8135	0.0016	0.172	0.0129	1	0.1865
Desert lands	0.001	0.7423	0.2467	0.01	1	0.2577
Cultivated lands	0.0146	0.0523	0.8071	0.126	1	0.1929
Urban Areas	0.0145	0.0125	0.5095	0.4635	1	0.5365
Total	0.8436	0.8087	1.7353	0.6124	4	
Gain	0.0301	0.0664	0.9282	0.1489		

Table 10. Transition probability matrix derived from LULC-classified categories in Sohag Governorate from 2013 to 2022.

	Probability of Changing from 2013 to 2022				Subtotals	
	Water Bodies	**Desert Lands**	**Cultivated Lands**	**Urban Areas**	**Total**	**Loss**
Water bodies	0.8237	0.0030	0.1642	0.0092	1	0.1763
Desert lands	0.0052	0.5909	0.2003	0.2036	1	0.4091
Cultivated lands	0.0362	0.0181	0.7820	0.1638	1	0.218
Urban Areas	0.0306	0.0289	0.4610	0.4796	1	0.5205
Total	0.8957	0.6409	1.6075	0.8559	4	
Gain	0.072	0.05	0.8255	0.3764		

For further understanding of the dynamic changes in LULC types in the Sohag Governorate, the annual change in these types was calculated for the three studied periods (1984–2002, 2002–2013, and 2013–2022), as shown in Table 11. According to the data in Table 11, cultivated lands increased annually by 8.5 km^2, 21.88 km^2, and 6.64 km^2 for the three studied periods, respectively. The greatest annual increase in cultivated land was recorded in the second period (2002–2013), during which increasing desert land reclamation activities were noticed. Furthermore, over the three time periods, the desert lands shrank by 12.06 km^2, 29.14 km^2, and 17.50 km^2 per year, respectively (Table 11). Moreover, the urban zones expanded at an annual rate of 3.76 km^2, 6.52 km^2, and 7.17 km^2 for the three studied periods, respectively. Water bodies decreased by 0.2 km^2 per year from 1984 to 2002, then increased by 0.73 km^2 in the second period, and the highest increase (3.69 km^2) occurred between 2013 and 2022 due to the construction and startup of wastewater treatment units in the study area (Table 11).

Table 11. Annual changes in LULC classes of Sohag Governorate.

Land Use	Annual Change km^2		
	1984–2002	**2002–2013**	**2013–2022**
Water bodies	−0.20	0.73	3.69
Desert lands	−12.06	−29.14	−17.50
Cultivated lands	8.50	21.88	6.64
Urban Areas	3.76	6.52	7.17

The results of the LULC class changes for different LULCs in the Sohag Governorate over the studied periods are displayed in Table 12. Furthermore, Figure 10 demonstrates the temporal distribution of LULC class changes in the Sohag Governorate in square kilometers over the years studied. The findings indicate that urban areas increased during the studied periods, and there was also a noticeable reduction in desert lands. The increase in urbanized areas can be attributed to population growth. The growth in urban areas (urbanization), which is associated with population increases, infrastructure development, and growing domestic product, is one of the primary drivers of LULC changes [24,123–127]. Moreover, cultivated lands, water bodies, and urban areas increased during the studied periods (Figure 10).

Table 12. Temporal distribution in km^2 of LULC distribution.

Land Use	1984		2002		Change from 1984 to 2002	2013		Change from 2002 to 2013	2022		Change from 2013 to 2022
	Areas										
	km^2	%	km^2	%	km^2	km^2	%	km^2	km^2	%	km^2
WB	64.2	2.2	60.6	2.0	−3.6	68.6	2.3	8.04	101.8	3.4	33.21
DL	1398.9	46.8	1181.8	39.5	−217.13	861.3	28.8	−320.5	703.8	23.6	−157.47
CL	1361.0	45.5	1514.0	50.7	152.99	1754.7	58.7	240.73	1814.5	60.7	59.73
Urban	165.0	5.5	232.8	7.8	67.74	304.5	10.2	71.73	369.0	12.3	64.52
Total	2989.1	100.0	2989.1	100.0		2989.1	100.0		2989.1	100.0	

WB = water bodies. DL = desert lands. CL = cultivated lands.

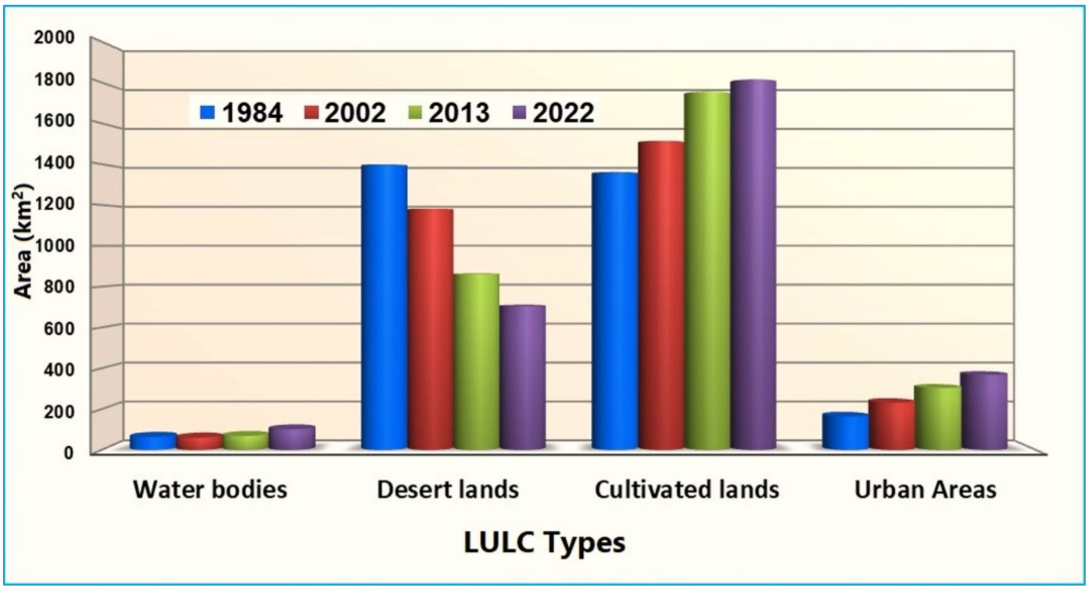

Figure 10. Temporal distribution of LULC change distribution in 1984, 2002, 2013, and 2022 (km^2).

3.5. CA-Markov Model Validation for Predicting Future LULC Scenarios

The Kappa coefficients for the quantity and location of correct cells were derived based on a comparison of the projected and classified LULC maps at a resolution of 30 m × 30 m for model validation employing the IDRISI program. According to k-indicator statistics for the LULCs in 2013, the $K_{standard}$, K_{no}, $K_{location}$, and $K_{location\text{-}strata}$ were 0.8703, 0.9142, 0.9336, and 0.9336, respectively, as shown in Table 13. Similarly, for 2022, k-indicator statistics revealed that the $K_{standard}$, K_{no}, $K_{location}$, and $K_{location\text{-}strata}$ were 0.8402, 0.8942, 0.9012, and 0.9012, respectively (Table 13). These findings demonstrated high agreement between the predicted and observed LULC maps for 2013 and 2022. This revealed that there were minor quantification and location errors between the projected and actual maps [104,128–130]. Therefore, employing the CA-Markov model can precisely specify the quantity and location of the LULC changes [100,118,128,131]. Furthermore, based on the satisfactory agreement between the predicted and observed LULC maps, the data in Table 13 and Figure 11 established that the accuracy appraisal of categorized data for 2013 and 2022 is satisfactory and reasonable for simulation and prediction applications [132]. As a result, the validated CA-Markov model is nearly perfect for simulating and projecting future LULC trends in arid land regions. These findings are in agreement with the results obtained from prior investigations [27,110,113,114,133,134].

Table 13. Kappa indices for 2013 and 2022.

K-Index	2013	2022
$K_{standard}$	0.8703	0.8402
K_{no}	0.9142	0.8942
$K_{location}$	0.9336	0.9012
$K_{location\ strata}$	0.9336	0.9012

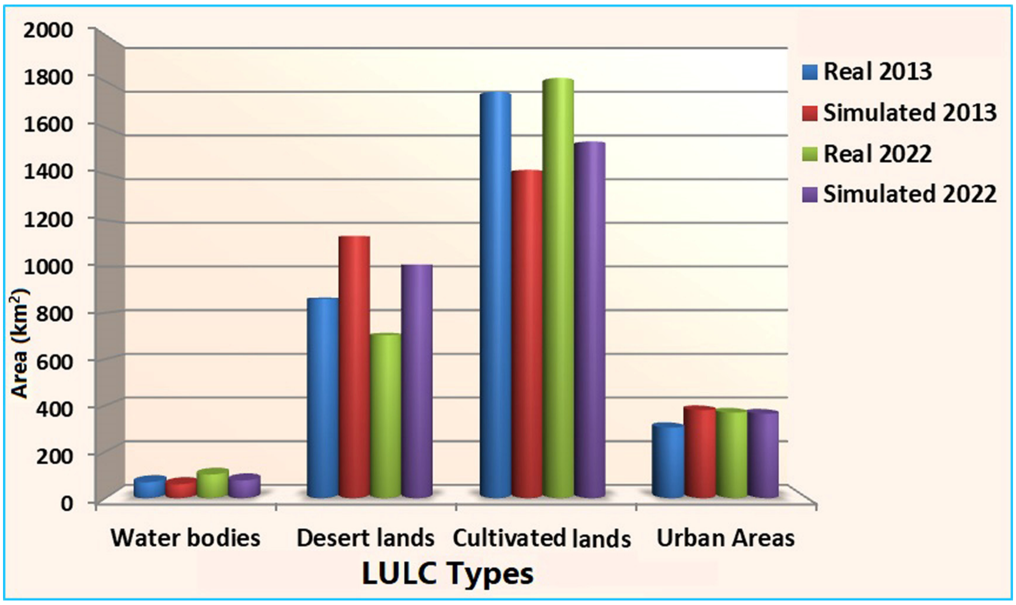

Figure 11. The comparison between simulated and actual LULCs in km^2 in 2013 and 2022.

3.6. Prediction of the Future LULC Scenarios

CA-Markov hybrid model was used to simulate and project future LULC trends for 2030, 2040, and 2050. The future scenarios of LULC classes for 2030, 2040, and 2050 are illustrated in Figure 12 as thematic maps of the predicted LULC spatial distributions. Furthermore, Table 14 displays the percentages and the areas in km^2 of the predicted LULC categories for 2030, 2040, and 2050. During all of the predicted periods, there would be increases in water bodies, cultivated lands, and urban areas. Desert lands, on the other hand, would decline in the study area during the same periods.

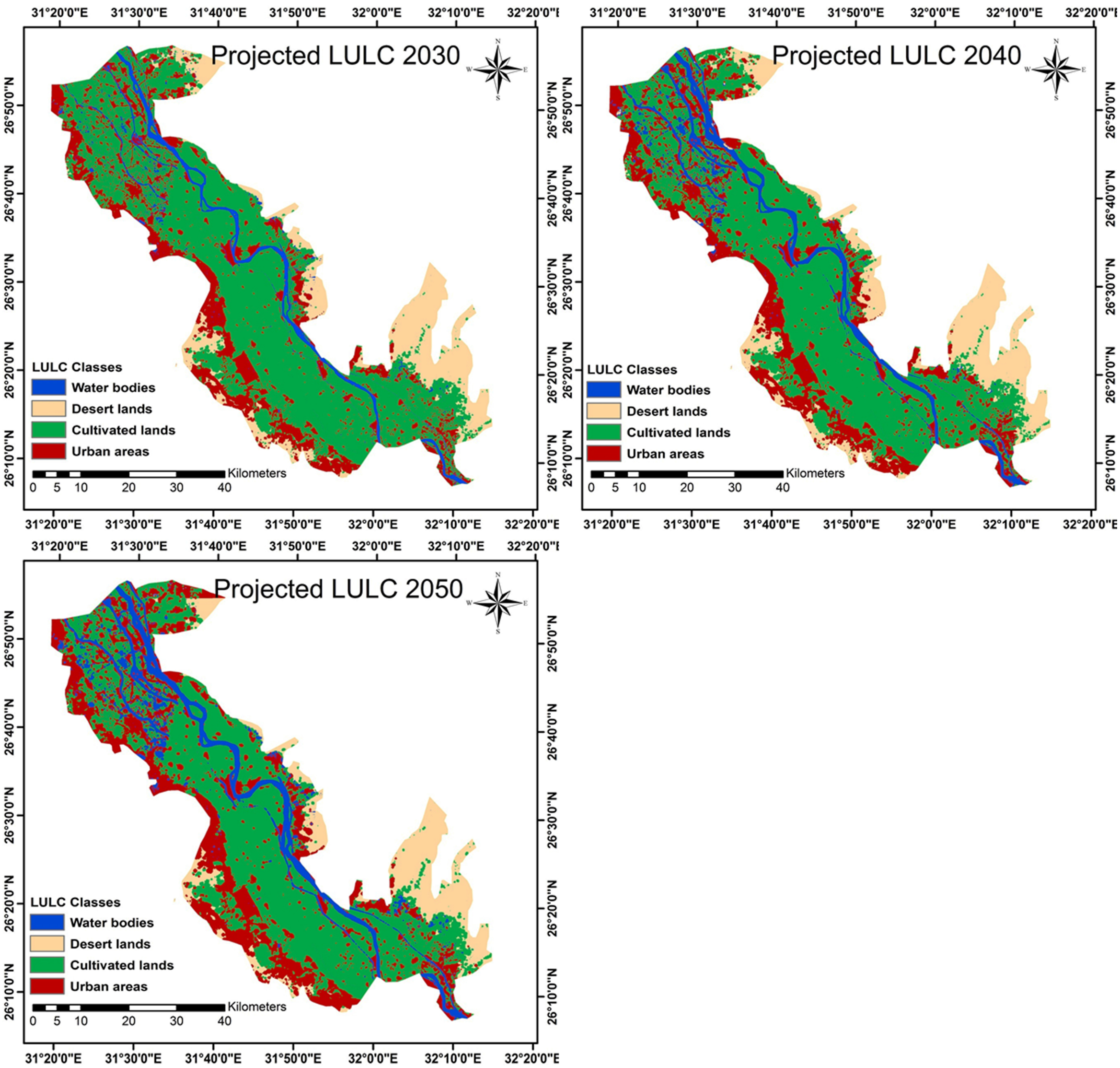

Figure 12. Spatial distribution maps of predicted LULCs for 2030, 2040, and 2050.

Table 14. The future predicted changes in areas of LULC classes in km^2.

Land Use	Projected 2030		Change from 2022 to 2030	Projected 2040		Change from 2030 to 2040	Projected 2050		Change from 2040 to 2050
	Areas								
	km^2	%	km^2	km^2	%	km^2	km^2	%	km^2
WB	164.44	5.50	62.64	194.1	6.49	29.66	200.8	6.72	6.7
DL	459.71	15.38	−244.09	312.4	10.45	−147.31	245.4	8.21	−67
CL	1746.63	58.43	−67.87	1808.3	60.50	61.67	1851.5	61.94	43.2
Urban	618.35	20.69	249.35	674.3	22.56	55.95	691.4	23.13	17.1
Total	2989.13	100	-	2989.1	100	-	2989.1	100	-

WB = water bodies. DL = desert lands. CL = cultivated lands.

The modeling results showed that built-up areas would increase significantly compared to their zones in the past and present, expanding from 165 km^2 (5.5%) in 1984 to 369 km^2 (12.3%) in 2022 to 618 km^2 (20.7%) in 2030 and 691 km^2 (23.1%) in 2050, as shown in Table 14. This predicted increase in urban areas might be related to the existing expansion in the built-up areas due to population growth [27,49,124,125,135]. Furthermore, cultivated lands would decrease slightly in 2030 by 67.9 km^2 and then increase slightly to reach 1851 km^2 (61.9%) in 2050 (Table 14). The predicted expansion in cultivated lands may be associated with the expansion of newly reclaimed soils due to ongoing land reclamation projects on arable lands. Moreover, desert land would continue to decline considerably from 703.8 km^2 (23.6%) in 2022 to 459.7 km^2 (15.4%), 312.4 km^2 (10.5%), and 245.4 km^2 (8.2%) in 2030, 2040, and 2050, respectively, as displayed in Table 14. Desert lands would be reduced due to urban sprawl and cultivated land expansion outside the Nile Valley through the reclamation of arable land in desert areas. Also, according to modeling results, the water bodies would increase slightly and gradually to reach 6.7% of the entire area of the study region in 2050.

Results of the simulation indicated that future scenarios represented by urban expansion growing, cultivated lands and water bodies increasing, and desert lands declining followed the past and current trends of LULC in the study region. This may be because the CA-Markov approach does not contain the variables that could influence or prevent the event of LULC changes. Thus, the resultant LULC trend updates in the coming years are expected to be linear. Projected maps can be identical to LULCs in 2030, 2040, and 2050 if the rate of the current changes is the same. However, because the current study was limited in its use of LULC change drivers and future LULC trends are unsure, additional factors should be considered to enrich our knowledge of LULC change trends [136]. Therefore, future research studies are required to assess the accuracy of these predicted scenarios and identify the variables that cause the LULC changes. Furthermore, this study's findings indicate that the Egyptian government should focus on LULC changes, specifically urban sprawl on old fertile farmlands, to ensure sustainable development in the study area.

Sustained farming should use resources in such a manner that they can renew their productivity potential while minimizing detrimental effects on ecosystems [137]. In this regard, FAO [4] has indicated that rapid population growth is causing increased land degradation to meet food demands. Overall, the current study provided a future vision of LULC trends that would be beneficial in land use management and offered a comprehensive understanding of ecosystem functions for establishing land use sustainability [138].

4. Conclusions

The current study was carried out to assess the performance of the CA-Markov hybrid model in predicting and modeling future LULC trends in arid regions using conventional remote sensing data. Therefore, this study focused on detecting and analyzing LULC change in the Sohag Governorate region over the different periods examined (1984, 2002, 2013, and 2022), as well as projecting and modeling future LULC trends for 2030, 2040, and 2050. The findings of the current study provided evidence that the CA-Markov hybrid model is an effective model for predicting and modeling the future LULC trends for 2030, 2040, and 2050 in the Sohag Governorate as an arid region using conventional remotely sensed data. Furthermore, results proved that the cellular automata filter was critical for improving the spatial distribution of various LULC classes in the study area. Concerning the accuracy assessment of the used model, an accuracy of greater than 70% was obtained in all stages. According to this study, CA-Markov modeling has delivered promisingly precise and reliable outcomes.

Moreover, the increased population and industrial and commercial activities in the Sohag Governorate are causing considerable urban sprawl. Although the newly reclaimed agricultural lands with moderate agricultural production potential are increasing, their productivity is insufficient to maintain sustainable food security, as the old farming lands with high production potential are dwindling. This investigation has shown that changing land use and land cover is a pervasive, rapid, and significant trend in Sohag Governorate. The results revealed that cultivated lands, built-up areas, and water bodies expanded from 1984 to 2022 at the expense of decreasing deserts. Furthermore, the most considerable increase in the area of cultivated lands and built-up occurred between 2002 and 2013, while the most significant decline in desert lands happened over the same period. The predicted 2030, 2040, and 2050 LULC results also presented that the trend from historical to future LULC change will be extended to be ongoing in the future.

Furthermore, this work exhibited the flexibility of integrating remote sensing, GIS, and CA-Markov modeling that can be utilized as an effective technique for mapping and tracking the LULC changes. Moreover, the change detection and prediction modeling of future LULC trends achieved in this work has some limitations. These limitations stem from the adoption of the CA-Markov approach, which does not contain the variables or factors that could influence or hinder the event of the LULC change in the study area. Therefore, future research studies are required to assess the accuracy of these expected scenarios and identify the variables that cause the LULC changes. Furthermore, future research is needed to evaluate the performance of the CA-Markov hybrid model with diverse land use classes in various arid regions. The Egyptian government should work hard to prevent the loss of productive old lands due to urban sprawl and to reclaim more unused arable land.

Author Contributions: Conceptualization, S.A.H.S., D.E.K., G.M., A.R.A.M., R.J.-B., O.D.K., M.E.F. and A.-r.A.M.; methodology, S.A.H.S., A.R.A.M., O.D.K., M.E.F. and A.-r.A.M.; software, S.A.H.S., D.E.K., A.R.A.M., O.D.K., M.E.F. and A.-r.A.M.; validation, S.A.H.S., D.E.K., G.M., A.R.A.M., R.J.-B., O.D.K., M.E.F. and A.-r.A.M.; formal analysis, S.A.H.S., A.R.A.M., M.E.F. and A.-r.A.M.; investigation, S.A.H.S., D.E.K., G.M, A.R.A.M., O.D.K., M.E.F. and A.-r.A.M.; resources, S.A.H.S., D.E.K., G.M., A.R.A.M., R.J.-B., O.D.K., M.E.F. and A.-r.A.M.; data curation, S.A.H.S., D.E.K., G.M., A.R.A.M., O.D.K., M.E.F. and A.-r.A.M.; writing—original draft preparation, S.A.H.S., A.R.A.M., O.D.K., M.E.F. and A.-r.A.M.; writing—review and editing, S.A.H.S., D.E.K., G.M., R.J.-B. and A.-r.A.M.; visualization, S.A.H.S., D.E.K., G.M., A.R.A.M., R.J.-B., O.D.K., M.E.F. and A.-r.A.M.; supervision, S.A.H.S., D.E.K. and A.-r.A.M.; project administration, S.A.H.S. and A.-r.A.M.; funding acquisition, S.A.H.S., D.E.K., A.R.A.M., G.M., R.J.-B., O.D.K., M.E.F. and A.-r.A.M. All authors have read and agreed to the published version of this manuscript.

Funding: This research received no external funding.

Data Availability Statement: Data are contained within the article.

Conflicts of Interest: The authors declare no conflict of interest.

References

1. Biro, K.; Pradhan, B.; Buchroithner, M.; Makeschin, F. Land use/land cover change analysis and its impact on soil properties in the northern part of Gadarif region, Sudan. *Land Degrad. Dev.* **2013**, *24*, 90–102. [CrossRef]
2. Ayele, A.; Tarekegn, K. The impact of urbanization expansion on agricultural land in Ethiopia: A review. *Environ. Socio-Econ. Stud.* **2020**, *8*, 73–80. [CrossRef]
3. Abdulaziz, A.M.; Hurtado, J.M.; Al-Douri, R. Application of multitemporal Landsat data to monitor land cover changes in the Eastern Nile Delta region, Egypt. *Int. J. Remote Sens.* **2009**, *30*, 2977–2996. [CrossRef]
4. FAO. *The Future of Food and Agriculture: Trends and Challenges*; FAO: Rome, Italy, 2017; ISBN 978-9-25109-551-5.
5. Calicioglu, O.; Flammini, A.; Bracco, S.; Bellù, L.; Sims, R. The Future Challenges of Food and Agriculture: An Integrated Analysis of Trends and Solutions. *Sustainability* **2019**, *11*, 222. [CrossRef]
6. Adepoju, M.O.; Millington, A.C.; Tansey, K.T. Land Use/Land Cover Change Detection in Metropolitan Lagos (Nigeria): 1984–2000. In Proceedings of the AASPRS 2006 Annual Conference, Reno, NV, USA, 1–5 May 2006.
7. Zabihi, M.; Moradi, H.; Gholamalifard, M.; Khaledi Darvishan, A.; Fürst, C. Landscape Management through Change Processes Monitoring in Iran. *Sustainability* **2020**, *12*, 1753. [CrossRef]
8. Dadashpoor, H.; Azizi, P.; Moghadasi, M. Analyzing spatial patterns, driving forces and predicting future growth scenarios for supporting sustainable urban growth: Evidence from Tabriz metropolitan area, Iran. *Sustain. Cities Soc.* **2019**, *47*, 101502. [CrossRef]
9. Dewan, A.M.; Yamaguchi, Y.; Ziaur Rahman, M. Dynamics of land use/cover changes and the analysis of landscape fragmentation in Dhaka Metropolitan, Bangladesh. *GeoJournal* **2012**, *77*, 315–330. [CrossRef]
10. Liu, J.; Zhang, Z.; Xu, X.; Kuang, W.; Zhou, W.; Zhang, S.; Li, R.; Yan, C.; Yu, D.; Wu, S.; et al. Spatial patterns and driving forces of land use change in China during the early 21st century. *J. Geogr. Sci.* **2010**, *20*, 483–494. [CrossRef]
11. Shi, G.; Jiang, N.; Yao, L. Land Use and Cover Change during the Rapid Economic Growth Period from 1990 to 2010: A Case Study of Shanghai. *Sustainability* **2018**, *10*, 426. [CrossRef]
12. Cihlar, J. Land cover mapping of large areas from satellites: Status and research priorities. *Int. J. Remote Sens.* **2000**, *21*, 1093–1114. [CrossRef]
13. Wang, S.Q.; Zheng, X.; Zang, X. Accuracy assessments of land use change simulation based on Markov-cellular automata model. *Procedia Environ. Sci.* **2012**, *13*, 1238–1245. [CrossRef]

14. Yan, W.Y.; Shaker, A.; El-Ashmawy, N. Urban land cover classification using airborne LiDAR data: A review. *Remote Sens. Environ.* **2015**, *158*, 295–310. [CrossRef]
15. Karki, S.; Thandar, A.M.; Uddin, K.; Tun, S.; Aye, W.M.; Aryal, K.; Kandel, P.; Chettri, N. Impact of land use land cover change on ecosystem services: A comparative analysis on observed data and people's perception in Inle Lake, Myanmar. *Environ. Syst. Res.* **2018**, *7*, 25. [CrossRef]
16. Long, H.; Tang, G.; Li, X.; Heilig, G.K. Socio–economic driving forces of land–use change in Kunshan, the Yangtze River Delta economic area of China. *J. Environ. Manag.* **2007**, *83*, 351–364. [CrossRef] [PubMed]
17. Ning, J.; Liu, J.; Kuang, W.; Xu, X.; Zhang, S.; Yan, C.; Li, R.; Wu, S.; Hu, Y.; Du, G.; et al. Spatiotemporal patterns and characteristics of land-use change in China during 2010–2015. *J. Geogr. Sci.* **2018**, *28*, 547–562. [CrossRef]
18. Prestele, R.; Alexander, P.; Rounsevell, M.D.A.; Arneth, A.; Calvin, K.; Doelman, J.; Eitelberg, D.A.; Engstrom, K.; Fujimori, S.; Hasegawa, T.; et al. Hotspots of uncertainty in land-use and land-cover change projections: A global-scale model comparison. *Glob. Change Biol.* **2016**, *22*, 3967–3983. [CrossRef]
19. Srivastava, P.K.; Han, D.; Rico-Ramirez, M.A.; Bray, M.; Islam, T. Selection of classification techniques for land use/land cover change investigation. *Adv. Space Res.* **2012**, *50*, 1250–1265. [CrossRef]
20. Degife, A.W.; Zabel, F.; Mauser, W. Assessing land use and land cover changes and agricultural farmland expansions in Gambella Region, Ethiopia, using Landsat 5 and Sentinel 2a multispectral data. *Heliyon* **2018**, *4*, e00919. [CrossRef]
21. Hou, H.; Wang, R.; Murayama, Y. Scenario-based modelling for urban sustainability focusing on changes in cropland under rapid urbanization: A case study of Hangzhou from 1990 to 2035. *Sci. Total Environ.* **2019**, *661*, 422–431. [CrossRef]
22. Motlagh, Z.K.; Lotfi, A.; Pourmanafi, S.; Ahmadizadeh, S.; Soffianian, A. Spatial modeling of land-use change in a rapidly urbanizing landscape in central Iran: Integration of remote sensing, CA-Markov, and landscape metrics. *Environ. Monit. Assess.* **2020**, *192*, 695. [CrossRef]
23. Ren, Y.; Lü, Y.; Comber, A.; Fu, B.; Harris, P.; Wu, L. Spatially explicit simulation of land use/land cover changes: Current coverage and future prospects. *Earth-Sci. Rev.* **2019**, *190*, 398–415. [CrossRef]
24. Berihun, M.L.; Tsunekawa, A.; Haregeweyn, N.; Meshesha, D.T.; Adgo, E.; Tsubo, M.; Masunaga, T.; Fenta, A.A.; Sultan, D.; Yibeltal, M. Exploring land use/land cover changes, drivers and their implications in contrasting agro-ecological environments of Ethiopia. *Land Use Policy* **2019**, *87*, 104052. [CrossRef]
25. Deng, X.; Huang, J.; Rozelle, S.; Uchida, E. Economic Growth and the Expansion of Urban Land in China. *Urban Stud.* **2010**, *47*, 813–843. [CrossRef]
26. Gan, B.R.; Liu, X.N.; Yang, X.G.; Wang, X.K.; Zhoua, J.W. The impact of human activities on the occurrence of mountain flood hazards: Lessons from the 17 August 2015 flash flood/debris flow event in Xuyong County, South-Western China. *Geomat. Nat. Hazards Risk* **2018**, *9*, 816–840. [CrossRef]
27. Munthali, M.G.; Mustak, S.; Adeola, A.; Botai, J.; Singh, S.K.; Davis, N. Modelling Land Use and Land Cover Dynamics of Dedza District of Malawi Using Hybrid Cellular Automata and Markov Model. *Remote Sens. Appl. Soc. Environ.* **2020**, *17*, 100276. [CrossRef]
28. You, H. Agricultural landscape dynamics in response to economic transition: Comparisons between different spatial planning zones in Ningbo region, China. *Land Use Policy* **2017**, *61*, 316–328. [CrossRef]
29. Apollonio, C.; Balacco, G.; Novelli, A.; Tarantino, E.; Piccinni, A.F. Land use change impact on flooding areas: The case study of Cervaro Basin (Italy). *Sustainability* **2016**, *8*, 996. [CrossRef]
30. Carvalho-Santos, C.; Nunes, J.P.; Monteiro, A.T.; Hein, L.; Honrado, J.P. Assessing the effects of land cover and future climate conditions on the provision of hydrological services in a medium-sized watershed of Portugal. *Hydrol. Process.* **2016**, *30*, 720–738. [CrossRef]
31. Hossain, F.; Moniruzzaman, M. Environmental Change Detection through Remote Sensing Technique: A Study of Rohingya Refugee Camp Area (Ukhia and Teknaf Sub-district), Cox's Bazar, Bangladesh. *Environ. Chall.* **2021**, *2*, 100024. [CrossRef]
32. Lambin, E.F.; Turner, B.L.; Geist, H.J.; Agbola, S.B.; Angelsen, A.; Bruce, J.W.; Coomes, O.T.; Dirzo, R.; Fischer, G.; Folke, C.; et al. The causes of land-use and land-cover change: Moving beyond the myths. *Glob. Environ. Change* **2001**, *11*, 261–269. [CrossRef]
33. Lambin, E.F.; Geist, H.J.; Lepers, E. Dynamics of Land-Use and Land-Cover Change in Tropical Regions. *Annu. Rev. Environ. Resour.* **2003**, *28*, 205–241. [CrossRef]
34. Mezger, G.; De Stefano, L.; Gonz, M. Analysis of the Evolution of Climatic and Hydrological Variables in the Tagus River Basin, Spain. *Water* **2022**, *14*, 818. [CrossRef]
35. Shang, X.; Jiang, X.; Jia, R.; Wei, C. Land use and climate change effects on surface runoff variations in the upper Heihe River basin. *Water* **2019**, *11*, 344. [CrossRef]
36. Sibanda, S.; Ahmed, F. Modelling historic and future land use/land cover changes and their impact on wetland area in Shashe sub-catchment, Zimbabwe. *Model. Earth Syst. Environ.* **2021**, *7*, 57–70. [CrossRef]
37. Yang, D.; Kanae, S.; Oki, T.; Koike, T.; Musiake, K. Global potential soil erosion with reference to land use and climate changes. *Hydrol. Process.* **2003**, *17*, 2913–2928. [CrossRef]
38. Behera, M.D.; Borate, S.N.; Panda, S.N.; Behera, P.R.; Roy, P.S. Modelling and analyzing the watershed dynamics using Cellular Automata (CA)–Markov model—A geo-information based approach. *J. Earth Syst. Sci.* **2012**, *121*, 1011–1024. [CrossRef]
39. Rahman, M.T.U.; Tabassum, F.; Rasheduzzaman, M.; Saba, H.; Sarkar, L.; Ferdous, J.; Uddin, S.Z.; Islam, A.Z. Temporal dynamics of land use/land cover change and its prediction using CA-ANN model for southwestern coastal Bangladesh. *Environ. Monit. Assess.* **2017**, *189*, 565. [CrossRef]

40. Armin, M.; Majidian, M.; Kheybari, V.G. Land Use/Land Cover Change Detection and Prediction in the Yasouj City Suburbs in Kohgiluyeh Va Boyerahmad Province in Iran. *Arid. Ecosyst.* **2020**, *10*, 203–210. [CrossRef]
41. Kotaridis, I.; Lazaridou, M. Environmental Change Detection Study in the Wider Area of Lignite Mines. *Civil Eng. Archit.* **2018**, *6*, 108–114. [CrossRef]
42. Hua, A.K. Land use land cover changes in detection of water quality: A study based on remote sensing and multivariate statistics. *J. Environ. Public Health* **2017**, *2017*, 7515130. [CrossRef]
43. Liping, C.; Yujun, S.; Saeed, S. Monitoring and predicting land use and land cover changes using remote sensing and GIS techniques—A case study of a hilly area, Jiangle, China. *PLoS ONE* **2018**, *13*, e0200493. [CrossRef] [PubMed]
44. Mannan, A.; Liu, J.; Zhongke, F.; Khan, T.U.; Saeed, S.; Mukete, B.; ChaoYong, S.; Yongxiang, F.; Ahmad, A.; Amir, M.; et al. Application of land-use/land cover changes in monitoring and projecting forest biomass carbon loss in Pakistan. *Glob. Ecol. Conserv.* **2019**, *17*, e00535. [CrossRef]
45. Rawat, J.S.; Kumar, M. Monitoring land use/cover change using remote sensing and GIS techniques: A case study of Hawalbagh block, district Almora, Uttarakhand, India. *Egypt. J. Remote Sens. Space Sci.* **2015**, *18*, 77–84. [CrossRef]
46. Nouri, J.; Gharagozlou, A.; Arjmandi, R.; Faryadi, S.; Adl, M. Predicting urban land use changes using a CA–Markov model. *Arab. J. Sci. Eng.* **2014**, *39*, 5565–5573. [CrossRef]
47. Yang, X.; Zheng, X.-Q.; Lv, L.-N. A spatiotemporal model of land use change based on ant colony optimization, Markov chain and cellular automata. *Ecol. Model.* **2012**, *233*, 11–19. [CrossRef]
48. Nath, B.; Wang, Z.; Ge, Y.; Islam, K.; Singh, R.P.; Niu, Z. Land Use and Land Cover Change Modeling and Future Potential Landscape Risk Assessment Using Markov-CA Model and Analytical Hierarchy Process. *ISPRS Int. J. Geo-Inf.* **2020**, *9*, 134. [CrossRef]
49. Maviza, A.; Ahmed, F. Analysis of past and future multi-temporal land use and land cover changes in the semi-arid UpperMzingwane sub-catchment in the Matabeleland south province of Zimbabwe. *Int. J. Remote Sens.* **2020**, *41*, 5206–5227. [CrossRef]
50. Hyandye, C.; Martz, L.W. A Markovian and cellular automata land-use change predictive model of the Usangu Catchment. *Int. J. Remote Sens.* **2017**, *38*, 64–81. [CrossRef]
51. Memarian, H.; Balasundram, S.K.; Talib, J.B.; Sung, C.T.B.; Sood, A.M.; Abbaspour, K. Validation of CA-Markov for simulation of land use and cover change in the Langat Basin, Malaysia. *Sci. Res.* **2012**, *4*, 542–554. [CrossRef]
52. Singh, S.K.; Mustak, S.; Srivastava, P.K.; Szabó, S.; Islam, T. Predicting spatial and decadal LULC changes through cellular automata Markov chain models using earth observation datasets and geo-information. *Environ. Process.* **2015**, *2*, 61–78. [CrossRef]
53. Weng, Q. Land use change analysis in the Zhujiang Delta of China using satellite remote sensing, GIS and stochastic modelling. *J. Environ. Manag.* **2002**, *64*, 273–284. [CrossRef] [PubMed]
54. Bashir, O.; Bangroo, S.A.; Guo, W.; Meraj, G.; Ayele, G.T.; Naikoo, N.B.; Shafai, S.; Singh, P.; Muslim, M.; Taddese, H.; et al. Simulating Spatiotemporal Changes in Land Use and Land Cover of the North-Western Himalayan Region Using Markov Chain Analysis. *Land* **2022**, *11*, 2276. [CrossRef]
55. Jia, W.; Gu, X.; Mi, X.; Yang, J.; Zang, W.; Liu, P.; Yan, J.; Zhu, H.; Zhang, X.; Zhang, Z. Multi-Scale Spatiotemporal Pattern Analysis and Simulation (MSPAS) Model with Driving Factors for Land Cover Change and Sustainable Development Goals: A Case Study of Nepal. *Remote Sens.* **2022**, *14*, 6295. [CrossRef]
56. Naboureh, A.; Moghaddam, M.H.R.; Feizizadeh, B.; Blaschke, T. An integrated object-based image analysis and CA-Markov model approach for modeling land use/land cover trends in the Sarab plain. *Arab. J. Geosci.* **2017**, *10*, 259. [CrossRef]
57. Pereira, C.O.; Escanilla-Minchel, R.; González, A.C.; Alcayaga, H.; Aguayo, M.; Arias, M.A.; Flores, A.N. Assessment of Future Land Use/Land Cover Scenarios on the Hydrology of a Coastal Basin in South-Central Chile. *Sustainability* **2022**, *14*, 16363. [CrossRef]
58. Wu, X.; Zhu, C.; Yu, J.; Zhai, L.; Zhang, H.; Yang, K.; Hou, X. Ecological Vulnerability in the Red Soil Erosion Area of Changting under Continuous Ecological Restoration: Spatiotemporal Dynamic Evolution and Prediction. *Forests* **2022**, *13*, 2136. [CrossRef]
59. Dey, N.N.; Al Rakib, A.; Kafy, A.A.; Raikwar, V. Geospatial Modelling of Changes in Land Use/Land Cover Dynamics Using Multi-Layer Perception Markov Chain Model in Rajshahi City, Bangladesh. *Environ. Chall.* **2021**, *4*, 100148. [CrossRef]
60. Fan, F.; Wang, Y.; Wang, Z. Temporal and spatial change detecting (1998–2003) and predicting of land use and land cover in Core corridor of Pearl River Delta (China) by using TM and ETM+ images. *Environ. Monit. Assess.* **2007**, *137*, 127–147. [CrossRef]
61. Hamad, R.; Balzter, H.; Kolo, K. Predicting land use/land cover changes using a CA-Markov model under two different scenarios. *Sustainability* **2018**, *10*, 3421. [CrossRef]
62. Yirsaw, E.; Wu, W.; Shi, X.; Temesgen, H.; Bekele, B. Land Use/Land Cover Change Modeling and the Prediction of Subsequent Changes in Ecosystem Service Values in a Coastal Area of China, the Su-Xi-Chang Region. *Sustainability* **2017**, *9*, 1204. [CrossRef]
63. Al-shalabi, M.; Billa, L.; Pradhan, B.; Mansor, S.; Al-Sharif, A.A.A. Modelling urban growth evolution and land-use changes using GIS based cellular automata and SLEUTH models: The case of Sana'a metropolitan city, Yemen. *Environ. Earth Sci.* **2013**, *70*, 425–437. [CrossRef]
64. Guan, D.; Li, H.; Inohae, T.; Su, W.; Nagaie, T.; Hokao, K. Modeling urban land use change by the integration of cellular automaton and markov model. *Ecol. Model.* **2011**, *222*, 3761–3772. [CrossRef]
65. Cheong, S.M.; Brown, D.; Kok, K.; López-Carr, D. Mixed Methods in Land Change Research: Towards Integration. *Trans. Inst. Br. Geogr.* **2012**, *37*, 8–12. [CrossRef]
66. Brown, D.G.; Walker, R.; Manson, S.; Seto, K.C. Modeling land use and land cover change. In *Land Change Science: Observing, Monitoring, and Understanding Trajectories of Change on the Earth's Surface*; Gutman, G., Janetos, A., Justice, C., Moran, E., Mustard, J., Rindfuss, R., Skole, D., Turner, B.L., II, Cochrane, M.A., Eds.; Kluwer Academic Publishers: Dordrecht, The Netherlands, 2004; pp. 395–409.

67. Bracchetti, L.; Carotenuto, L.; Catorci, A. Land-cover changes in a remote area of central Apennines (Italy) and management directions. *Landsc. Urban Plan.* **2012**, *104*, 157–170. [CrossRef]
68. Tattoni, C.; Ciolli, M.; Ferretti, F. The fate of priority areas for conservation in protected areas: A fine-scale markov chain approach. *Environ. Manag.* **2011**, *47*, 263–278. [CrossRef] [PubMed]
69. Belay, T.; Mengistu, D.A. Impacts of land use/land cover and climate changes on soil erosion in Muga watershed, Upper Blue Nile basin (Abay), Ethiopia. *Ecol. Process.* **2021**, *10*, 68. [CrossRef]
70. Soil Survey Staff. *Keys to Soil Taxonomy*, 12th ed.; USDA-Natural Resources Conservation Service: Washington, DC, USA, 2014.
71. Hansen, M.C.; Defries, R.S.; Townshend, J.R.G.; Sohlberg, R. Global land cover classification at 1 km spatial resolution using a classification tree approach. *Int. J. Remote Sens.* **2000**, *21*, 1331–1364. [CrossRef]
72. Jensen, J.R. *Introductory Digital Image Processing*, 3rd ed.; Prentice Hall: Upper Saddle River, NJ, USA, 2005.
73. Weier, J.; Herring, D. *Measuring Vegetation: NDVI and EVI*; NASA Earth Observatory: Washington, DC, USA, 2000.
74. Xu, H.Q. Modification of normalised difference water index (NDWI) to enhance open water features in remotely sensed imagery. *Int. J. Remote Sens.* **2006**, *27*, 3025–3033. [CrossRef]
75. Zha, Y.; Gao, J.; Ni, S. Use of normalized difference built-up index in automatically mapping urban areas from TM imagery. *Int. J. Remote Sens.* **2003**, *24*, 583–594. [CrossRef]
76. Zhao, H.; Chen, X. Use of normalized difference bareness index in quickly mapping bare areas from TM/ETM+. In Proceedings of the 2005 IEEE International Geoscience and Remote Sensing Symposium, Seoul, Republic of Korea, 25–29 July 2005; Volume 3, pp. 1666–1668. [CrossRef]
77. Ibharim, N.; Mustapha, M.A.; Lihan, T.; Mazlan, A. Mapping mangrove changes in the Matang Mangrove Forest using multi temporal satellite imageries. *Ocean Coast. Manag.* **2015**, *114*, 64–76. [CrossRef]
78. Lin, C.; Wu, C.-C.; Tsogt, K.; Ouyang, Y.-C.; Chang, C.-I. Effects of atmospheric correction and pansharpening on LULC classification accuracy using WorldView-2 imagery. *Inf. Processing Agric.* **2015**, *2*, 25–36. [CrossRef]
79. Congalton, R.G.; Green, K. *Assessing the Accuracy of Remotely Sensed Data*; CRC Press: Boca Raton, FL, USA, 2009; ISBN 0-87-37198-67.
80. Sulieman, H.M. Mapping and modelling of vegetation changes in the Southern Gadarif region, Sudan, using remote sensing. Ph.D. Thesis, Dresden University of Technology, Dresden, Germany, 2008.
81. Zhang, Z.; Liu, S.; Wei, J.; Xu, J.; Guo, W.; Bao, W.; Jiang, Z. Mass change of glaciers in Muztag Ata–Kongur Tagh, Eastern Pamir, China from 1971/76 to 2013/14 as derived from remote sensing data. *PLoS ONE* **2016**, *11*, e0147327. [CrossRef] [PubMed]
82. Anderson, J.R.; Hardy, E.E.; Roach, J.T.; Witmer, R.E. *A Land Use and Land Cover Classification System for Use with Remote Sensor Data*; Government Printing Office: Washington, DC, USA, 1976.
83. Stehman, S. Estimating the kappa coefficient and its variance under stratified random sampling. *Photogramm. Eng. Remote Sens.* **1996**, *62*, 401–407.
84. Kumar, S.; Radhakrishnan, N.; Mathew, S. Land use change modelling using a Markov model and remote sensing. *Geomat. Nat. Hazards Risk* **2014**, *5*, 145–156. [CrossRef]
85. Guan, D.; Gao, W.; Watari, K.; Fukahori, H. Land use change of Kitakyushu based on landscape ecology and Markov model. *J. Geogr. Sci.* **2008**, *18*, 455–468. [CrossRef]
86. Chen, Y.; Li, X.; Liu, X.; Ai, B. Analyzing land-cover change and corresponding impacts on carbon budget in a fast developing sub-tropical region by integrating MODIS and Landsat TM/ETM+ images. *Appl. Geogr.* **2013**, *45*, 10–21. [CrossRef]
87. Myint, S.W.; Wang, L. Multicriteria decision approach for land use land cover change using Markov chain analysis and a cellular automata approach. *Can. J. Remote Sens.* **2006**, *32*, 390–404. [CrossRef]
88. Biswas, M.; Banerji, S.; Mitra, D. Land-use–land-cover change detection and application of Markov model: A case study of Eastern part of Kolkata. *Environ. Dev. Sustain.* **2019**, *22*, 4341–4360. [CrossRef]
89. Hu, Y.; Zheng, Y.; Zheng, X. Simulation of land-use scenarios for Beijing using CLUE-S and Markov composite models. *Chin. Geogr. Sci.* **2013**, *23*, 92–100. [CrossRef]
90. Sang, L.; Zhang, C.; Yang, J.; Zhu, D.; Yun, W. Simulation of land use spatial pattern of towns and villages based on CA-Markov model. *Math. Comput. Model.* **2011**, *54*, 938–943. [CrossRef]
91. Wu, N.; Silva, E. Artificial intelligence solutions for urban land dynamics: A review. *J. Plan. Lit.* **2010**, *24*, 246–265. [CrossRef]
92. Eastman, J.R. *IDRISI Selva Tutorial*; Clark University: Worcester, MA, USA, 2012; pp. 267–275.
93. Aliani, H.; Malmir, M.; Sourodi, M.; Kafaky, S.B. Change detection and prediction of urban land use changes by CA–Markov model (case study: Talesh County). *Environ. Earth Sci.* **2019**, *78*, 546. [CrossRef]
94. Nadoushan, M.A.; Soffianian, A.; Alebrahim, A. Modeling land use/cover changes by the combination of markov chain and cellular automata markov (CA-Markov) models. *J. Earth Environ. Health Sci.* **2015**, *1*, 16–21. [CrossRef]
95. Clarke, K.C.; Hoppen, S.; Gaydos, L. A self-modifying cellular automaton model of historical urbanization in the San Francisco Bay area. Environ. *Plan. B Plan. Des.* **1997**, *24*, 247–261. [CrossRef]
96. Yang, Q.S.; Li, X.; Shi, X. Cellular automata for simulating land use changes based on support vector machines. *Comput. Geosci.* **2008**, *34*, 592–602. [CrossRef]
97. Ma, C.; Zhang, G.; Zhang, X.; Zhao, Y.; Li, H. Application of Markov model in wetland change dynamics in Tianjin Coastal Area, China. *Procedia Environ. Sci.* **2012**, *13*, 252–262. [CrossRef]
98. Irwin, E.G.; Jayaprakash, C.; Munroe, D.K. Towards a comprehensive framework for modeling urban spatial dynamics. *Landsc. Ecol.* **2009**, *24*, 1223–1236. [CrossRef]

99. He, D.; Zhou, J.; Gao, W.; Guo, H.Y.U.S.; Liu, Y. An integrated CA–markov model for dynamic simulation of land use change in Lake Dianchi watershed. *Acta Sci. Nat. Univ. Pekin.* **2014**, *50*, 1095–1105. [CrossRef]
100. Keshtkar, H.; Voigt, W. A spatiotemporal analysis of landscape change using an integrated Markov chain and cellular automata models. *Model. Earth Syst. Environ.* **2016**, *2*, 1–13. [CrossRef]
101. Liang, X.; Liu, X.; Li, D.; Zhao, H.; Chen, G. Urban growth simulation by incorporating planning policies into a CA–based future land–use simulation model. *Int. J. Geogr. Inf. Sci.* **2018**, *32*, 2294–2316. [CrossRef]
102. Aksoy, H.; Kaptan, S. Simulation of future forest and land use/cover changes (2019–2039) using the cellular automata-Markov model. *Geocarto Int.* **2020**, *37*, 1183–1202. [CrossRef]
103. Wang, R.; Murayama, Y. Change of Land Use/Cover in Tianjin City Based on the Markov and Cellular Automata Models. *ISPRS Int. J. Geo-Inf.* **2017**, *6*, 150. [CrossRef]
104. Singh, S.K.; Laari, P.B.; Mustak, S.; Srivastava, P.K.; Szabó, S. Modelling of land use land cover change using earth observation data-sets of Tons River Basin, Madhya Pradesh, India. *Geocarto Int.* **2018**, *33*, 1202–1222. [CrossRef]
105. Tali, J.A.; Divya, S.; Murthy, K. Influence of urbanization on the land use change: A case study of Srinagar City. *Am. J. Res. Comm.* **2013**, *1*, 271–283.
106. Eastman, J.R. *IDRISI Taiga Guide to GIS and Image Processing*; Clark Labs Clark University: Worcester, MA, USA, 2009.
107. Subedi, P.; Subedi, K.; Thapa, B. Application of a Hybrid Cellular Automaton—Markov (CA-Markov) Model in Land-Use Change Prediction: A Case Study of Saddle Creek Drainage Basin, Florida. *Appl. Ecol. Environ. Sci.* **2013**, *1*, 126–132. [CrossRef]
108. Pan, S.; Liu, D.; Wang, Z.; Zhao, Q.; Zou, H.; Hou, Y.; Liu, P.; Xiong, L. Runoff Responses to Climate and Land Use/Cover Changes under Future Scenarios. *Water* **2017**, *9*, 475. [CrossRef]
109. Tilahun, A.; Teferie, B. Accuracy assessment of land use land cover classification using Google Earth. *Am. J. Environ. Prot.* **2015**, *4*, 193–198. [CrossRef]
110. Da Cunha, E.R.; Santos, C.A.G.; da Silva, R.M.; Bacani, V.M.; Teodoro, P.E.; Panachuki, E.; de Souza Oliveira, N. Mapping LULC types in the Cerrado-Atlantic Forest ecotone region using a Landsat time series and object-based image approach: A case study of the Prata River Basin, Mato Grosso do Sul, Brazil. *Environ. Monit. Assess.* **2020**, *192*, 136. [CrossRef]
111. Li, X.; Liu, X.; Yu, L. A systematic sensitivity analysis of constrained cellular automata model for urban growth simulation based on different transition rules. *Int. J. Geogr. Inf. Syst.* **2014**, *28*, 1317–1335. [CrossRef]
112. Rimal, B.; Zhang, L.; Keshtkar, H.; Haack, B.N.; Rijal, S.; Zhang, P. Land Use/Land Cover Dynamics and Modeling of Urban Land Expansion by the Integration of Cellular Automata and Markov Chain. *ISPRS Int. J. Geo-Inf.* **2018**, *7*, 154. [CrossRef]
113. Abd El-Hamid, H.T.; El-Alfy, M.A.; Elnaggar, A. Prediction of future situation of land use/cover change and modeling sensitivity to pollution in Edku Lake. Egypt based on geospatial analyses. *GeoJournal* **2020**, *86*, 1895–1913. [CrossRef]
114. Abd El-Hamid, H.T.A.; Nour-Eldin, H.; Rebouh, N.Y.; El-Zeiny, A.M. Past and Future Changes of Land Use/Land Cover and the Potential Impact on Ecosystem Services Value of Damietta Governorate, Egypt. *Land* **2022**, *11*, 2169. [CrossRef]
115. Abd El-Kawy, O.R.; Rød, J.K.; Ismail, H.A.; Suliman, A.S. Land use and land cover change detection in the western Nile delta of Egypt using remote sensing data. *Appl. Geogr.* **2011**, *31*, 483–494. [CrossRef]
116. Elagouz, M.; Abou-Shleel, S.; Belal, A.; El-Mohandes, M. Detection of land use/cover change in Egyptian Nile Delta using remote sensing. *Egypt. J. Remote Sens. Space Sci.* **2019**, *23*, 57–62. [CrossRef]
117. El-Zeiny, A.M.; Effat, H.A. Environmental monitoring of spatiotemporal change in land use/land cover and its impact on land surface temperature in El-Fayoum governorate, Egypt. *Remote Sens. Appl. Soc. Environ.* **2017**, *8*, 266–277. [CrossRef]
118. Halmy, M.W.A.; Gessler, P.E.; Hicke, J.A.; Salem, B.B. Land use/land cover change detection and prediction in the north-western coastal desert of Egypt using Markov-CA. *Appl. Geogr.* **2015**, *63*, 101–112. [CrossRef]
119. Kamel, M. Monitoring of Land Use and Land Cover Change Detection Using Multi-temporal Remote Sensing and Time Series Analysis of Qena-Luxor Governorates (QLGs), Egypt. *J. Indian Soc. Remote Sens.* **2020**, *48*, 1767–1785. [CrossRef]
120. Mohamed, E.S.; Baroudy, A.A.E.; El-beshbeshy, T.; Emam, M.; Belal, A.A.; Elfadaly, A.; Aldosari, A.A.; Ali, A.M.; Lasaponara, R. Vis-NIR Spectroscopy and Satellite Landsat-8 OLI Data to Map Soil Nutrients in Arid Conditions: A Case Study of the Northwest Coast of Egypt. *Remote Sens.* **2020**, *12*, 3716. [CrossRef]
121. Said, M.E.S.; Ali, A.M.; Borin, M.; Abd-Elmabod, S.K.; Aldosari, A.A.; Khalil, M.M.N.; Abdel-Fattah, M.K. On the Use of Multivariate Analysis and Land Evaluation for Potential Agricultural Development of the Northwestern Coast of Egypt. *Agronomy* **2020**, *10*, 1318. [CrossRef]
122. Biondini, M.; Kandus, P. Transition matrix analysis of land-cover change in the accretion area of the Lower Delta of the Paraná River (Argentina) reveals two succession pathways. *Wetlands* **2006**, *26*, 981–991. [CrossRef]
123. Bai, X.; Chen, J.; Shi, P. Landscape Urbanization and Economic Growth in China: Positive Feedbacks and Sustainability Dilemmas. *Environ. Sci. Technol.* **2012**, *46*, 132–139. [CrossRef]
124. Huang, G.; Jiang, Y. Urbanization and Socioeconomic Development in Inner Mongolia in 2000 and 2010: A GIS Analysis. *Sustainability* **2017**, *9*, 235. [CrossRef]
125. Deng, X.; Huang, J.; Rozelle, S.; Zhang, J.; Li, Z. Impact of urbanization on cultivated land changes in China. *Land Use Policy* **2015**, *45*, 1–7. [CrossRef]
126. Marques, A.; Martins, I.S.; Kastner, T.; Plutzar, C.; Theurl, M.C.; Eisenmenger, N.; Huijbregts, M.A.J.; Wood, R.; Stadler, K.; Bruckner, M.; et al. Increasing impacts of land use on biodiversity and carbon sequestration driven by population and economic growth. *Nat. Ecol. Evol.* **2019**, *3*, 628–637. [CrossRef] [PubMed]

127. Pandey, B.K.; Khare, D. Analyzing and modeling of a large river basin dynamics applying integrated cellular automata and Markov model. *Environ. Earth Sci.* **2017**, *76*, 779. [CrossRef]
128. Gashaw, T.; Tulu, T.; Argaw, M.; Worqlul, A.W. Evaluation and prediction of land use/land cover changes in the Andassa watershed, Blue Nile Basin, Ethiopia. *Environ. Syst. Res.* **2017**, *6*, 17. [CrossRef]
129. Pontius, G.J.; Schneider, L.C. Land-cover change model validation by an ROC method for the Ipswich watershed, Massachusetts, USA. *Agric. Ecosyst. Environ.* **2001**, *85*, 239–248. [CrossRef]
130. Pontius, R.; Millones, M. Death to Kappa: Birth of quantity disagreement and allocation disagreement for accuracy assessment. *Int. J. Remote Sens.* **2011**, *32*, 4407–4429. [CrossRef]
131. Luo, G.; Amuti, T.; Zhu, L.; Mambetov, B.T.; Maisupova, B.; Zhang, C. Dynamics of landscape patterns in an inland river delta of Central Asia based on a cellular automata-Markov model. *Reg. Environ. Chang.* **2015**, *15*, 277–289. [CrossRef]
132. Mondal, M.S.; Sharma, N.; Kappas, M.; Garg, P.K. CA Markov modeling of land use land cover change predictions and effect of numerical iterations, image interval (time steps) on prediction results. Int. Arch. Photogramm. *Remote Sens. Spatial Inf. Sci.* **2020**, *43*, 713–720. [CrossRef]
133. Huang, Y.C.; Yang, B.G.; Wang, M.; Liu, B.W.; Yang, X.D. Analysis of the future land cover change in Beijing using CA-Markov chain model. *Environ. Earth Sci.* **2020**, *79*, 60. [CrossRef]
134. Khwarahm, N.R.; Najmaddin, P.M.; Ararat, K.; Qader, S. Past and future prediction of land cover land use change based on earth observation data by the CA–Markov model: A case study from Duhok governorate, Iraq. *Arab. J. Geosci.* **2021**, *14*, 1–14. [CrossRef]
135. Gidey, E.; Dikinya, O.; Sebego, R.; Segosebe, E.; Zenebe, A. Cellular automata and Markov Chain (CA_Markov) model-based predictions of future land use and land cover scenarios (2015–2033) in Raya, northern Ethiopia. *Modeling Earth Syst. Environ.* **2017**, *3*, 1245–1262. [CrossRef]
136. Matlhodi, B.; Kenabatho, P.K.; Parida, B.P.; Maphanyane, J.G. Analysis of the Future Land Use Land Cover Changes in the Gaborone Dam Catchment Using CA-Markov Model: Implications on Water Resources. *Remote Sens.* **2021**, *13*, 2427. [CrossRef]
137. Brodt, S.; Six, J.; Feenstra, G.; Ingels, C.; Campbell, D. Sustainable Agriculture. *Nat. Educ. Knowl.* **2011**, *3*, 1.
138. Dewan, A.; Yamaguchi, Y. Land use and land cover change in Greater Dhaka, Bangladesh: Using remote sensing to promote sustainable urbanization. *Appl. Geogr.* **2009**, *29*, 390–401. [CrossRef]